



HAL
open science

Combining Fast 2D NMR Methods and Oriented Media

Philippe Lesot, Olivier Lafon

► **To cite this version:**

Philippe Lesot, Olivier Lafon. Combining Fast 2D NMR Methods and Oriented Media. Jean-Nicolas Dumez; Patrick Giraudeau. Fast 2D Solution-state NMR: Concepts and Applications, 1, The Royal Society of Chemistry, 2023, 978-1-83916-400-2. 10.1039/BK9781839168062-00441 . hal-04207389

HAL Id: hal-04207389

<https://hal.science/hal-04207389>

Submitted on 14 Sep 2023

HAL is a multi-disciplinary open access archive for the deposit and dissemination of scientific research documents, whether they are published or not. The documents may come from teaching and research institutions in France or abroad, or from public or private research centers.

L'archive ouverte pluridisciplinaire **HAL**, est destinée au dépôt et à la diffusion de documents scientifiques de niveau recherche, publiés ou non, émanant des établissements d'enseignement et de recherche français ou étrangers, des laboratoires publics ou privés.

Combining fast 2D-NMR Methods and Oriented Media

Philippe Lesot^{a,b,*}  and Olivier Lafon^c 

^a Université Paris-Saclay, Institut Chimie Moléculaire et des Matériaux d'Orsay, ICMMO, UMR CNRS 8182, Equipe RMN en Milieu Orienté, Site BPC (HM1), 17-19 Avenue des Sciences, 91400 Orsay, France.

^b Centre National de la Recherche Scientifique (CNRS), 3 rue Michel Ange, F-75016 Paris, France.

^c Université de Lille, CNRS, Centrale Lille, Université Artois, UMR CNRS 8181, Unité de Catalyse et Chimie du Solide, UCCS, F-59000 Lille, France.

*Corresponding author: Philippe Lesot

*Corresponding email address: philippe.lesot@universite-paris-saclay.fr

ABSTRACT:

NMR in oriented samples (anisotropic solvents) offers access to informative residual order-dependent NMR interactions, including chemical shift anisotropies (RCSAs), dipolar couplings (RDCs), and quadrupolar couplings (RQCs), while preserving high spectral resolution. The analysis of these spectra often requires two-dimensional (2D) NMR experiments due to these additional anisotropic interactions. In addition, accelerated 2D NMR experiments can be essential for particular investigations, including *in-situ* monitoring of chemical reactions or the observation of dilute isotopes, e.g. ^2H and ^{13}C , since the stability of oriented phases is limited in time and the magnetic field, B_0 , can drift in the absence of ^2H lock. We provide here an overview of these fast 2D-NMR experiments in anisotropic media. These developments have benefited from those for isotropic solutions, such as fast pulsing techniques enhancing the polarization, sparse sampling, Hadamard spectroscopy or spatial encoding. Nevertheless, fast 2D-NMR in mesophases and solids present particular challenges, since these 2D spectra usually display lower signal-to-noise ratio, non-Lorentzian lineshapes, lower spectral resolution and wider spectral width than their counterparts for isotropic solutions. We discuss here the advantages and limitations of the various approaches, which have been applied for the fast 2D-NMR spectra of mesophases and solids.

Keywords:

Anisotropic NMR, Fast 2D NMR, Polypeptide mesophases, NUS, Covariance, Compressed sensing, Ultrafast NMR, Hadamard spectroscopy, Fast pulsing

Orcid:

PL  : <https://orcid.org/000-0002-5811-7530>

OL  : <https://orcid.org/0000-0002-5214-4060>

15.1. Introduction

Over the past four decades, multidimensional (*nD*) nuclear magnetic resonance (**NMR**) experiments on liquids or solids have become major analytical tools for a wide range of applications, including health, energy, food, advanced materials, environment and cultural heritage.^{1,2,3} NMR experiments of these different states of matter allow us to access different NMR interactions and hence, they provide complementary insights into the atomic-level structure and dynamics. Furthermore, NMR of intermediate states of matter between liquids and solids, such as (chiral or achiral) lyotropic liquid crystals or gels, offers additional capabilities by leveraging the anisotropy and fluidity of these phases.^{4,5,6}

NMR in oriented solvents has become an essential tool to determine molecular structures, the enantiomeric purity of chiral mixtures, and the intra-molecular isotopic distribution, but also to study dynamic processes, such as chemical or conformational exchanges as well as to monitor chemical reactions.^{5,6} 2D NMR spectra of anisotropic media are generally acquired using the approach proposed by Jean Jeener.^{7,8} The 1D NMR experiment is repeated while varying a delay, the indirect evolution period, t_1 . The 2D NMR spectra are reconstructed using the discrete Fourier transform (**FT**)⁹ which requires constant t_1 increments, *i.e.* uniform sampling (**US**). Nevertheless, the acquisition of these 2D NMR spectra can be long, which is notably a serious limitation for the *in situ* monitoring of chemical reactions, studying mesophases or molecules of limited stability, and recording ^2H NMR spectra at natural abundance level, without any lock system of the static magnetic field, \mathbf{B}_0 .

A wide range of alternative sampling approaches have been introduced for accelerating the acquisition of multidimensional NMR experiments in isotropic phases, and among them some have been experimentally tested with anisotropic solvents. In this Chapter, an overview of various approaches when using aligning media (mainly polypeptide-based chiral lyotropic liquid crystals (**LLC**)) is presented.

15.2. Principle and concepts of fast 2D-NMR in anisotropic media

In this section below, we present the minimal basic concepts of NMR in (chiral) oriented solvents, the main 2D NMR experiments employed for the study of these samples, in particular for ^2H quadrupolar isotope, which has nuclear spin $I = 1$, and some potential applications of fast 2D NMR in these peculiar media.^{5,6}

15.2.1. Basics of NMR in (chiral) liquid crystals or aligned gels

Oriented media are intermediate states of the matter between liquids and solids (see **Figure 15.1a**), where solute molecules can be either strongly aligned, *e.g.* in thermotropics ($S \approx 10^{-1} - 10^{-3}$), weakly oriented, *e.g.* in lyotropic solvents ($S \approx 10^{-3} - 10^{-4}$), or very weakly oriented, *e.g.* in gels ($S \approx 10^{-3} - 10^{-5}$). For instance, a homogenous molecular alignment in a magnetic field \mathbf{B}_0

can be achieved using: i) small-sized mesogenic molecules (thermotropic liquid crystals (**LC**))¹⁰, ii) polymer-based LLCs.^{5,6} (see **Figure 15.1b**), and iii) stretched or compressed gels (see **Figure 15.1c**).^{11,12} This molecular alignment allows the measurement of anisotropic NMR interactions, such as residual chemical shift anisotropies (**RCSAs**, $\Delta\sigma$), residual intramolecular dipolar couplings (**RDCs**, D) or residual quadrupolar couplings for spins $I \geq 1$ (**RQCs**, $\Delta\nu_Q$), which are all averaged to zero by random molecular tumbling in isotropic solutions.^{5,6,10} These residual anisotropic NMR interactions provide therefore unique insights into the structure, the dynamics and the orientation of the molecules (analyte or solvent). Nevertheless, compared to solids, the molecules rotate and diffuse rapidly at the NMR time scale. These fast motions average out most intermolecular dipolar couplings, which simplifies the NMR spectra. Furthermore, in weakly (or very weakly) ordering solvents, such as (chiral or achiral) LLCs and gels^{11,12}, the magnitude of these residual anisotropic NMR interactions is comparable to or lower than that of isotropic NMR interactions, such as isotropic chemical shifts and J -couplings. Hence, guest molecules in these media exhibit generally high-resolution NMR spectra (more or less complex depending on the number of interacting spins), and the linewidths of their NMR peaks do not exceed a few Hertz.

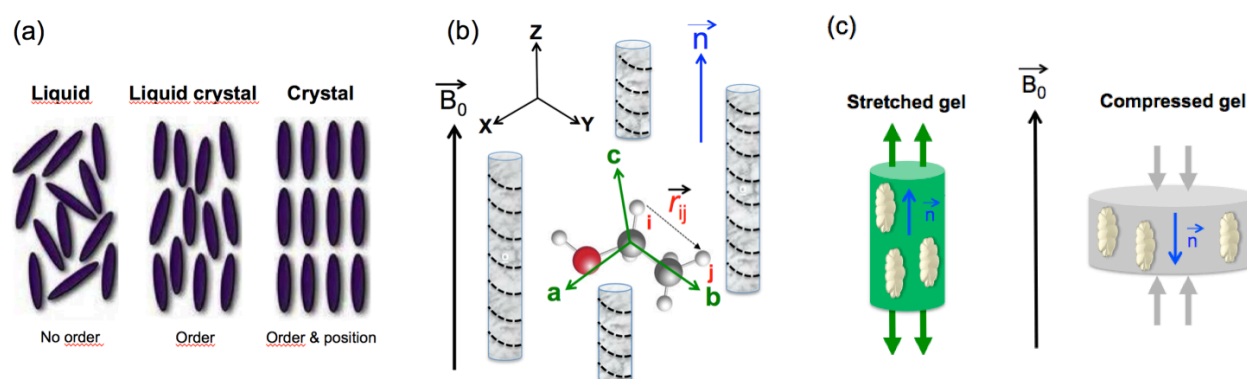


Figure 15.1 Schematic description of: **(a)** the molecular order in isotropic liquids (no order), in (nematic) liquid crystals (displaying only orientational order) and in crystalline solids (featuring both orientational and positional orders); **(b)** of a solute embedded in a chiral polymer-based LLC with a phase director, \vec{n} , aligned with \vec{B}_0 in the laboratory frame (X, Y, Z). The solute alignment can be described by using an axis system attached to the molecule (a, b, c); **(c)** of stretched and compressed gels inducing a molecular order with respect to \vec{B}_0 . **Reprinted from Ref. 6 with permission from [Wiley].**

Interestingly, in chiral oriented media, such as chiral crystal liquids (**CLCs**) made of poly- γ -benzyl-L-glutamate (**PBLG**) (see **Figure 15.1b**) or chiral thermotropics or chiral gels, two enantiomers of chiral analytes or enantiotopic elements (atoms, groups of atoms or directions) in prochiral molecules adopt distinct molecular orientations on average, which leads to distinct anisotropic NMR interactions.^{6,13} Mathematical descriptors of the orientational order and the anisotropic NMR interactions are summarized in **Table 15.1**. More detailed descriptions of these interactions can be found in the literature.^{5,6,10,13}

Table 15.1. Key equations describing the orientational order and the three main anisotropic NMR interactions.^{5,6,13}

| Notations | Equations and details | Eq. | |
|--|--|---|--------|
| (Molecular) Saupe's order matrix $S_{\alpha\beta}$ / no unit | $S_{\alpha\beta} = \frac{1}{2} \langle 3 \cos \theta_Z^\alpha \cos \theta_Z^\beta - \delta_{\alpha\beta} \rangle$ | - $\delta_{\alpha\beta}$ is the Kronecker delta with $\delta_{\alpha\beta} = 1$ if $\alpha = \beta$, and 0 if $\alpha \neq \beta$. - θ_Z^α or θ_Z^β is the angle between the molecular axis α or $\beta = a, b$ and c , and the Z axis of laboratory frame (aligned with \mathbf{B}_0). | (15.1) |
| (Internuclear) local order parameter S_{ij} / no unit | $S_{ij} = \sum_{\alpha, \beta = a, b, c} \cos \theta_{ij}^\alpha \cos \theta_{ij}^\beta S_{\alpha\beta}$ | - $\theta_{ij}^{\alpha \text{ or } \beta}$ is the angle between an internuclear vector (\mathbf{r}_{ij}) and the molecular axis α or $\beta = a, b$ or c . | (15.2) |
| (Internuclear) local order parameter S_{ij} / no unit | $S_{ij} = \frac{1}{2} \langle 3 \cos^2 \theta_{ij}^{B_0} - 1 \rangle$ | - $\theta_{ij}^{B_0}$ is the angle between an internuclear vector (\mathbf{r}_{ij}) and the \mathbf{B}_0 axis. | (15.3) |
| Residual dipolar coupling (RDC) D_{ij} / Hz | $D_{ij} = -k_{ij} \left\langle \frac{S_{ij}}{r_{ij}^3} \right\rangle$ $k_{ij} = \left(\frac{\mu_0}{4\pi} \right) \times \left(\frac{h\gamma_i\gamma_j}{4\pi^2} \right)$ | - γ_i and γ_j are the gyromagnetic ratios of (two homo- or heteronuclei, i and j , respectively). - r_{ij} is the internuclear vector between nuclei i and j . - μ_0 is the vacuum permittivity constant - h is the Planck constant. | (15.4) |
| Residual chemical shift anisotropy ^a (RCSA) σ_i^{aniso} / Hz | $\sigma_i^{\text{aniso}} = \frac{2}{3} \sum_{\alpha, \beta = a, b, c} \sigma_{\alpha\beta i} S_{\alpha\beta}$ $\sigma_i^{\text{iso}} = \frac{1}{3} (\sigma_{aa_i}^{\text{iso}} + \sigma_{bb_i}^{\text{iso}} + \sigma_{cc_i}^{\text{iso}})$ $\nu_i^{\text{iso}} = -\frac{\gamma_i}{2\pi} (1 - \sigma_i^{\text{iso}} - \sigma_i^{\text{aniso}}) B_0$ | - σ_i^{iso} and σ_i^{aniso} are the electronic isotropic and anisotropic shielding constants, respectively. - $\sigma_{aa_i}^{\text{iso}}$, $\sigma_{bb_i}^{\text{iso}}$ and $\sigma_{cc_i}^{\text{iso}}$ are the diagonal elements of the electronic shielding tensor for the nucleus i . | (15.5) |
| Residual quadrupolar coupling ^b (RQC, for $I = 1$) $\Delta\nu_{Q_i}$ / Hz | $\Delta\nu_{Q_i} = \frac{3}{2} K_{C-D_i} S_{C-D_i}$ $K_{C-D_i} = \frac{eQ_{D_i} V_{C-D_i}}{h}$ $S_{C-D_i} = \frac{1}{2} \langle 3 \cos^2 \theta_{C-D_i}^{B_0} - 1 \rangle$ | - K_{C-D_i} is the ^2H quadrupolar coupling constant (QCC). - Q_{D_i} is the ^2H nuclear electric quadrupolar moment. - $V_{C-D_i} = e q_{C-D_i}$ is the electric field gradient (EFG) along the $C-D_i$ bond. | (15.6) |
| Total spin-spin coupling ^c T_{ij} or T_{ii} / Hz | $T_{ij} = J_{ij} + 2D_{ij} \text{ (AX spin system)}$ $T_{ii} = 3D_{ii} \text{ (A}_2 \text{ or A}_3 \text{ spin system)}$ | - J_{ij} is the homo- or heteronuclear scalar coupling. - A_2 or A_3 spin systems is associated with two (or three) isogamous and isochronous nuclei (e.g. an isolated CH_2 or CH_3 group). | (15.7) |

^a The RCSA modifies the chemical shift of nuclei in anisotropic media (ν_i^{aniso}) compared to the ν_i^{iso} value measured in isotropic solvent. This term can be positive or negative. ^b RQCs are only detected for nuclei with spin $I \geq 1$. Here the equations are given for a ^2H nucleus ($I = 1$) subject to an axially symmetric electric field gradient. ^c The notations, T_{ij}

and T_{ii} , are used to denote the total spin-spin coupling between two inequivalent and equivalent (isogamous and isochronous) nuclei, respectively.

The anisotropic NMR interactions can be measured for various NMR-active isotopes. In particular, all organic molecules contain ^1H , ^2H and ^{13}C nuclei.¹³ ^1H , ^2H and ^{13}C NMR experiments in anisotropic media differ notably by their receptivity, their resolution and their sensitivity to molecular orientational order. Their advantages and limitations are summarized in **Table 15.2**.

Table 15.2. Main advantages and limitations of ^1H , ^2H and ^{13}C NMR experiments at natural abundance level in (chiral) anisotropic media.

| Isotope (spin I) | Advantages | Limitations |
|--|--|---|
| ^1H ($I = \frac{1}{2}$) | <ul style="list-style-type: none"> - High receptivity owing to 99.985% natural abundance level and high gyromagnetic ratio - Small amount of analyte requested (< 10 mg) | <ul style="list-style-type: none"> - Complex 1D spectra with limited resolution owing to long-range $T(^1\text{H}-^1\text{H})$, narrow chemical shift range (0 - 15 ppm) and homonuclear 2nd-order effects (AB, ABC, AA'MM'X system, ...) - Small $^1\text{H}-^1\text{H}$ RDCs (0 to 30 Hz) and very small ^1H-RCSAs (0 to 5 Hz) |
| ^2H ($I = 1$) | <ul style="list-style-type: none"> - Large magnitude of ^2H-RQC values (0-1000 Hz), which are sensitive to small order difference - Simple 2D spectra to analyze owing to the lack of $^2\text{H}-^2\text{H}$ couplings (highly dilute spin) - Detection of enantio- and diastereo-isotopomers | <ul style="list-style-type: none"> - Low receptivity owing to very low abundance ($1.5 \times 10^{-2}\%$) and low gyromagnetic ratio ($\gamma(^2\text{H}) = \gamma(^1\text{H})/6.515$) - Hence, large amount of analyte requested (20-100 mg) - Weak chemical shift distribution (0 - 15 ppm) - Small magnitude of ^2H-RCSAs (0 to 2 Hz) |
| ^{13}C ($I = \frac{1}{2}$) | <ul style="list-style-type: none"> - Large chemical shift range (0 - 250 ppm) - Simple ^1H-decoupled ^{13}C NMR spectra owing to the lack of $^{13}\text{C}-^{13}\text{C}$ couplings (very highly dilute spin) - Large magnitude of RCSAs (sp/sp² atoms) - Moderate magnitude of ($^{13}\text{C}-^1\text{H}$)-RDCs (0 - 100 Hz) | <ul style="list-style-type: none"> - Moderate receptivity owing to moderate gyromagnetic ratio ($\gamma(^{13}\text{C}) = \gamma(^1\text{H})/3.99$) and low natural abundance (1.1%) and long T_1 relaxation time (sp-hybridized and quaternary ^{13}C) - Medium amount of analyte requested (10 - 20 mg) - Complex ^1H-coupled ^{13}C NMR spectra owing to heteronuclear 2nd-order effects on $^{13}\text{CH}_2$ group (ABX system, X: ^{13}C) |

15.2.2. 2D NMR in anisotropic media

1D NMR spectra of oriented analytes are often more difficult to interpret and assign than those of isotropic solutions because of the anisotropic NMR interactions, which can be comparable to the isotropic NMR interactions and produce additional splittings of the resonances as well as second-order effects. Hence, several efficient 2D NMR experiments have been introduced to improve the resolution of these spectra and to facilitate their analysis as well as the assignment of resonances. These experiments, which separate the NMR signals along different spectral

dimensions and refocus the unwanted NMR interactions, include notably: i) the 2D homo- or hetero-selective refocusing experiment (SERF/HetSERF),^{14,15,16} ii) ¹H-¹³C heteronuclear correlation experiments, such as clip-clap HSQC,^{17,18} which have been used to measure (¹H-¹³C)-RDCs,^{19,20} iii) ²H autocorrelation experiments, such as **Q-COSY** (or **Q-COSY Fz**) **Q-resolved** (or **Q-resolved Fz**) or **Q-DQD** (see pulse sequences shown in **Figure 15.2**),^{21,22,23} which correlate the two components of the ²H quadrupolar doublets ($l = 1$) and facilitate the assignment of ²H NMR spectra and the measurement of ²H-RQCs,^{24,25,26} and iv) ²H-¹³C heteronuclear correlation experiments (²H-¹³C HETCOR or *R*-NASDAC experiments, as well as the Q.E.COSY experiments which allows the determination of the sign of ²H-RQCs relative to the ²H-¹³C total spin coupling.^{27,28,29}

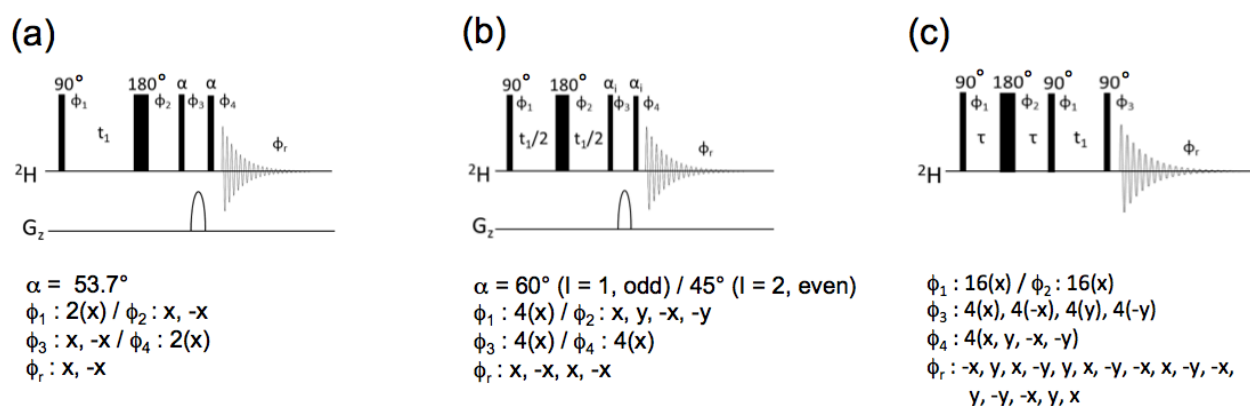


Figure 15.2 (a,b,c) Pulse schemes of conventional ²H QUOSY 2D sequences (Q-COSY, Q-resolved and Q-DQ, respectively). Hard radiofrequency (RF) pulses and pulse field gradients (PFG) are noted as rectangular block and a half ellipsoid, respectively. The z-filter block ($P\alpha$ - G_z - $P\alpha$) in Q-COSY and Q-resolved sequences allow recording pure absorption 2D spectra. When required, ¹H composite pulse decoupling (CPD) sequence such as WALTZ-16 can be applied during these sequences to eliminate the couplings with protons (not shown here). **Adapted from Ref. 30 with permission from [Wiley].**

The ²H autocorrelation and ²H-¹³C heteronuclear correlation experiments in anisotropic media are referred as homo- and hetero-nuclear quadrupole ordered spectroscopy (**QUOSY**). Four examples of experimental *n*D QUOSY spectra are displayed in **Figure 15.3**. These QUOSY experiments are notably useful for the analysis of perdeuterated molecules or isotopically normal (natural abundance level) analytes.^{24,25}

15.2.3. Application domains of fast NMR in anisotropic systems

Like for isotropic solutions, the acceleration of multidimensional NMR experiments recorded in oriented media is useful for two reasons: i) to reduce the experimental times (T_{exp}) of long 2D/3D NMR experiments while preserving exploitable spectral resolution, and ii) to record 2D experiments in less than a few seconds (or below) for monitoring fast dynamic processes, such as chemical reactions in oriented media.

15.2.3.1 Detection of nuclei with low natural abundance

Anisotropic homo- or hetero-nuclear nD NMR spectra involving low abundant nuclei, such as 2H ($1.55 \times 10^{-2}\%$) or ^{13}C (1.1%), generally require several hours (10 - 15 h) of data acquisition, even when using high-field NMR spectrometers equipped with cryogenic probes (see [Figure 15.3a,b,c](#)).³¹ These long experimental times can impede the study of compounds with limited stability and hence, short lifetimes. The duration of these experiments can also be limited by the macroscopic stability of the orienting media, which does not exceed 15 - 18 h for the majority of polypeptide-based LLCs, as well as by the B_0 field drift in the case of NAD QUOSY experiments, which are carried out without any lock to detect the 2H signals. In this context, some fast 2D NMR techniques, such as fast pulsing techniques enhancing polarization and sparse sampling, can enhance the NMR sensitivity by allowing a more frequent sampling of the signal, when its amplitude is large.^{17,32} This sensitivity gain is advantageous to reduce the experimental times for the detection of diluted solutes and isotopes of low natural abundance, such as 2H or ^{13}C or both, in isotopically unmodified analytes, as discussed below in [Section 15.3](#).

15.2.3.2 Chemical reaction monitoring

As a quantitative technique, NMR spectroscopy is a useful tool to monitor chemical reactions in real time. This approach consists in the measurement as function of reaction time of the integrated NMR intensities of the various species, which are proportional to their concentrations in the investigated sample. NMR at high³³ or low magnetic field^{34,35} can be employed to monitor reactions in isotropic solvents under batch or flow conditions, *i.e.* in a standard NMR tube or using a flow NMR probe or cell.³⁶ For these experiments, the gain in resolution provided by 2D NMR spectra is also very useful to identify the different species formed in the course of the reaction and to separate their signals so that their integrated intensities can be estimated in a reliable way. Nevertheless, conventional 2D experiments, even on isotopes of high receptivity, such as protons, require several minutes to sample properly the indirect evolution period, t_1 . Therefore, techniques to accelerate the acquisition of 2D NMR spectra are highly useful for reaction monitoring. Readers wishing to learn more about the use of fast 2D NMR to monitor chemical reactions are invited to read **Chapter 9** of this book.

NMR in oriented media is also a promising tool to monitor chemical reactions. NMR in thermotropic (achiral) liquid crystals has been first used to investigate the influence of the solvent anisotropy on the fate of the reaction.³⁷ Another advantage of oriented media (chiral or not) is the use of anisotropic NMR interactions to obtain new insights into the progress of a reaction. In particular, it has been shown that 2H - $\{^1H\}$ NMR in CLCs could be advantageously employed to monitor the conversion between deuterated enantiomers. This capability was

demonstrated through the investigation of the racemization of a scalemic mixture of alanine- d_3 ([3,3,3- $^2\text{H}_3$]-alanine in IUPAC nomenclature) containing an excess of the L-enantiomer by the **AR** enzyme in DNA-based solution.³⁸ Here the enantiodiscrimination properties of DNA helices (made of 200-300 base pairs) oriented in water result in different orientations for each

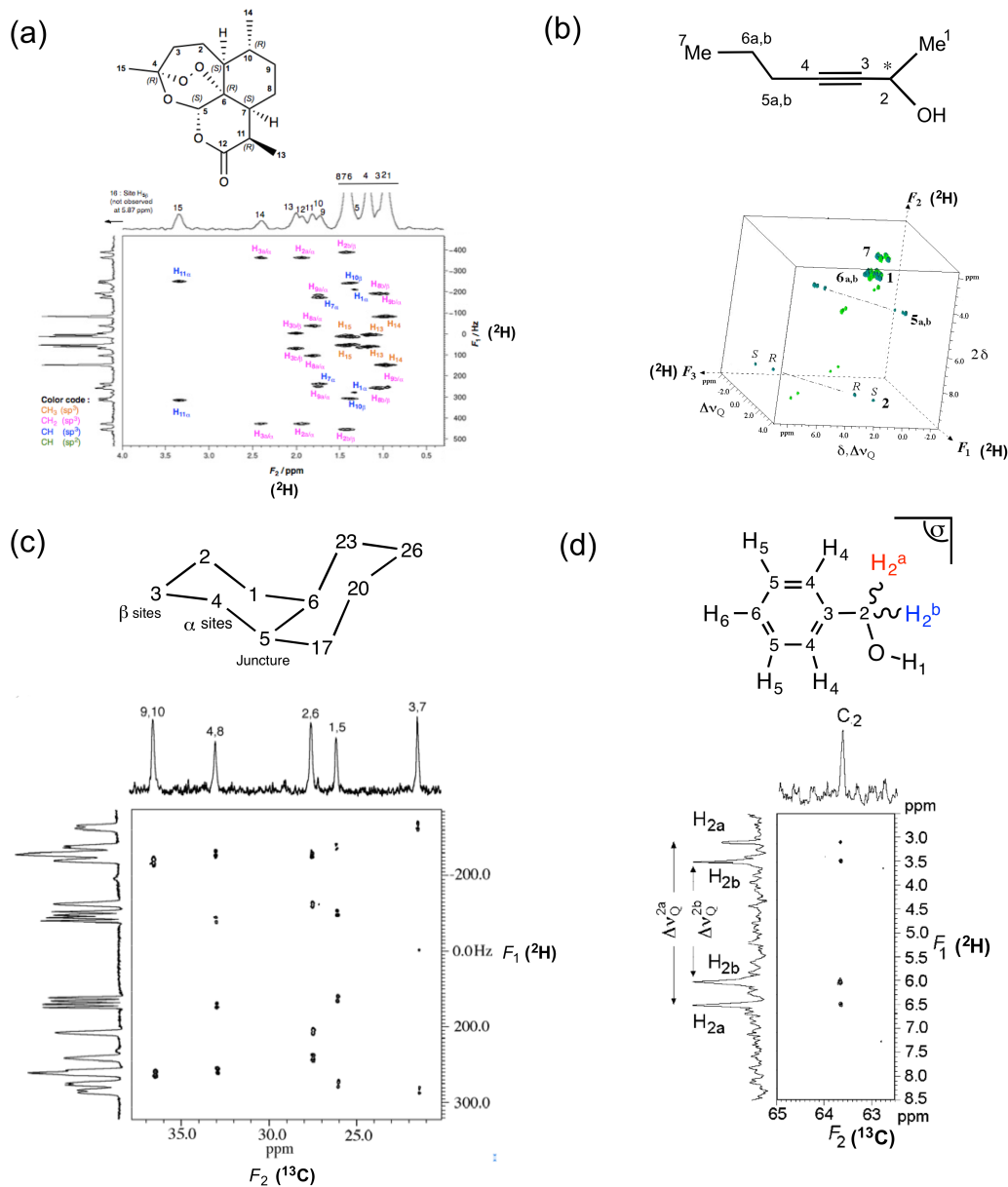


Figure 15.3 Four examples of QUOSY 2D spectra in PBLG-based CLCs recorded in more than 10 hours. **(a)** 92.1 MHz tilted NAD- $\{^1\text{H}\}$ Q-resolved Fz of artemisin. **(b)** NAD- $\{^1\text{H}\}$ Q-DQ 3D spectrum of (\pm)-but-2-yn-1-ol. The spectral information for each of the three dimensions is shown on the 3D spectrum. **(c)** 9.4 T anisotropic $^2\text{H} \rightarrow ^{13}\text{C}$ HETCOR 2D spectrum of *cis*- $^2\text{H}_{18}$ decalin recorded at low temperature (241 K). **(d)** 21.1 T *R*-NASDAC 2D spectrum of isotopically unmodified benzyl alcohol showing the first detection of ^2H - ^{13}C enantio-isotopomers. **Adapted from Ref. 23, 25, 26 and 28 with permission from [ACS] and [Elsevier].**

enantiomer, and hence, distinct ^2H -RQCs for the [3,3,3- $^2\text{H}_3$]-alanine isomers (see **Figure 15-4**). After the addition of AR in the medium, the evolution of the relative amounts of the two enantiomers is monitored by recording 1D ^2H - $\{^1\text{H}\}$ NMR spectra at different time

intervals. Interestingly, $^2\text{H}\{-^1\text{H}\}$ NMR of deuterated substrates provides a simple analysis of enantiomeric ^2H signals. As seen in **Figure 15-4a**, the intensity of the L-enantiomer signals decreases, whereas that of the D-enantiomer increases, and hence, the enantiomeric excess (*ee*) vanishes after a few hours. The simulation of the evolutions of the integrated intensities as a function of reaction time using reversible Michaelis-Merten kinetic model allows the determination of the rate constants for the reaction of L- and D-enantiomers with AR (k_{catL} and k_{catD}). These constants differ because of distinct Michaelis constants K_{M} and $K_{\text{M}'}$.³⁸ The values of k_{catL} and k_{catD} rates obtained with this tool were consistent with previous values determined using circular dichroism, which confirmed the reliability and the accuracy of the proposed approach.

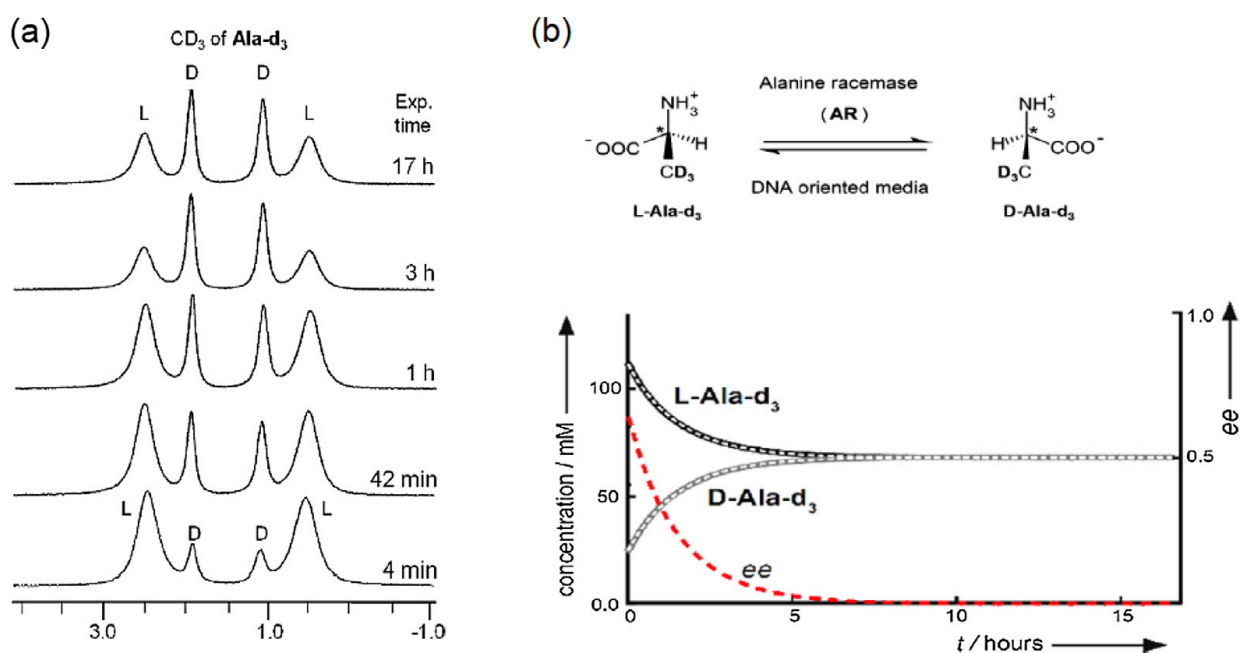


Figure 15.4 (a) Evolution of 1D $^2\text{H}\{-^1\text{H}\}$ NMR spectra as a function of time, plotted with same intensity scale of $[\text{3,3,3-}^2\text{H}_3]\text{-L-alanine}$ and $[\text{3,3,3-}^2\text{H}_3]\text{-D-alanine}$ mixture dissolved in DNA-based LLC containing the AR enzyme. The time $t = 0$ corresponds to the dissolution of AR in the LLC. The broader width of ^2H signals of L-enantiomer stems from larger $^2\text{H}\text{-}^2\text{H}$ total couplings. (b) (top) Alanine racemase catalyses the racemization of $[\text{3,3,3-}^2\text{H}_3]\text{-alanine}$. (bottom) Evolution of experimental (black and grey continuous lines) and fitted (white dashed lines) concentrations of deuterated L- and D-alanine as well as *ee* (red dashed line) versus reaction time. Adapted from Ref. 38 with permission from [ACS].

For very fast and complex chemical transformations, the rapid acquisition of 2D NMR spectra in oriented media become essential, since it prevents significant signal overlap and facilitates the separation of the signals of the different species (reactants, intermediates and products). Furthermore, as explained above, 2D NMR spectra are often required for the assignment of NMR spectra in oriented media since anisotropic NMR interactions increase the number of resonances and complicate the spectral analysis. In particular, the rapid acquisition of 2D ^2H QUOSY spectra will be beneficial for monitoring reactions involving perdeuterated reactants in LLCs. This approach will allow the simultaneous measurement of a much larger number of ^2H -

RQCs, compared to mono-deuterated reactants, and hence, will provide additional information about the changes in the molecular structure, and notably the stereochemistry, during the course of a reaction.

15.2.4. Possible approaches for fast 2D NMR in oriented media

The acquisition of n D NMR spectra of solutes in isotropic solutions can be significantly accelerated by various strategies. Among them, we can mention: i) the enhancement of the initial longitudinal magnetization using high magnetic fields³⁹ or DNP,^{40,41,42} ii) the shortening of the recycle delay (T_R) using paramagnetic relaxation agents^{43,44}, band-selective ^1H or ^{13}C excitation and/or optimized flip angles (well-known as Ernst angle), such as the SOFAST, BEST, ALSOFAST and ASAP approaches,^{17,45,46,47,48} iii) the use of more sensitive detection, including the indirect detection *via* nuclei with high gyromagnetic ratio, such as ^1H or ^{19}F ,⁴⁹ or the reduction of the electronic noise using cryogenic NMR probes,³¹ iv) the reduction of the number of increments in the indirect evolution period by a non-uniform sampling (**NUS**) of data (known also sparse sampling),⁵⁰ and v) the use of spatial encoding, also called ultrafast (**UF**) or single-scan NMR⁵¹ or frequency-domain sampling⁵² instead of the approach proposed by Jeener.⁷ Among these techniques, high-magnetic fields, cryogenic NMR probes, indirect detection, NUS, UF, ALSOFAST and ASAP fast pulsing approaches¹⁷ have been applied to accelerate the acquisition of 2D NMR spectra in oriented media,⁵³ We review in the following sections the advances related to the use of alternative sampling methods, including NUS, UF, and fast pulsing.

15.3. NUS and anisotropic ^2H NMR

15.3.1. NUS acquisition

As mentioned above, 2D NMR spectra are usually acquired using US, *i.e.* a constant increment of the indirect evolution period, Δt_1 , and analyzed using 2D FT with respect to t_1 and the acquisition period, t_2 . The length of the increment, Δt_1 , is fixed by the indirect spectral width, SW_1 , according to the Nyquist condition,

$$\Delta t_1 = 1/(SW_1), \quad (15.8)$$

whereas the maximal evolution period, $t_{1\text{max}}$, determines the achievable resolution along the indirect frequency dimension.³² A 2D NMR spectrum is usually highly redundant since it contains about 10^6 points, whereas the number of signals is lower than 10^2 and the lineshape of

each signal can be described by approximately 10 points along the indirect dimension, i.e. less than 10^3 points corresponds to signals.

Therefore, a first approach to accelerate the acquisition of nD spectra consists in the omission of some of the Δt_1 increments, i.e. variable Δt_1 increments are employed. This NUS only samples a subset of the t_1 increments, which are normally sampled in US at the Nyquist frequency (see [Figure 15.5](#)). In particular, in random NUS, the interval between two consecutive sampled indirect evolution times is random. This randomness leads to a wider dispersion of sampling artifacts along the indirect dimension.⁵⁰ Compared to truncated US, in which the sampling is stopped before the signals have decayed to zero, NUS allows preserving the resolution by acquiring signals for long t_1 periods, while reducing the number of sampled points. For NUS, the spectral width along the indirect dimension and the resolution are determined by the minimal t_1 increment and the longest sampled t_1 period, whereas the number of sampled points depends on the number of points containing signal in the 2D spectrum, and hence, on the type of 2D experiments and the investigated sample.⁵⁴ Usually NUS retains between 25 and 50% of the points sampled in US, both depending on the 2D experiment and the sample studied.⁵⁵

Furthermore, the sampling density of NUS can be adjusted to the envelope of the signal to enhance the sensitivity. For instance, exponentially biased random NUS can be employed for exponentially decaying NMR signals.⁵⁴ For a spectrum displaying Lorentzian lineshapes, optimal sensitivity is achieved for an exponential sampling density with a decay rate, which is twice faster than that of the signal envelope.^{32,54,55,56} This optimal decay rate results from a compromise between the suppression of the noise and the appearance of sampling artefacts. For such optimal sampling density, the sensitivity enhancement with respect to US is equal to 1.5-2 for $1.2/\text{FWHM} \leq t_{1\text{max}} \leq 1.5/\text{FWHM}$, where FWHM is the full-width at half maximum along the indirect dimension.³²

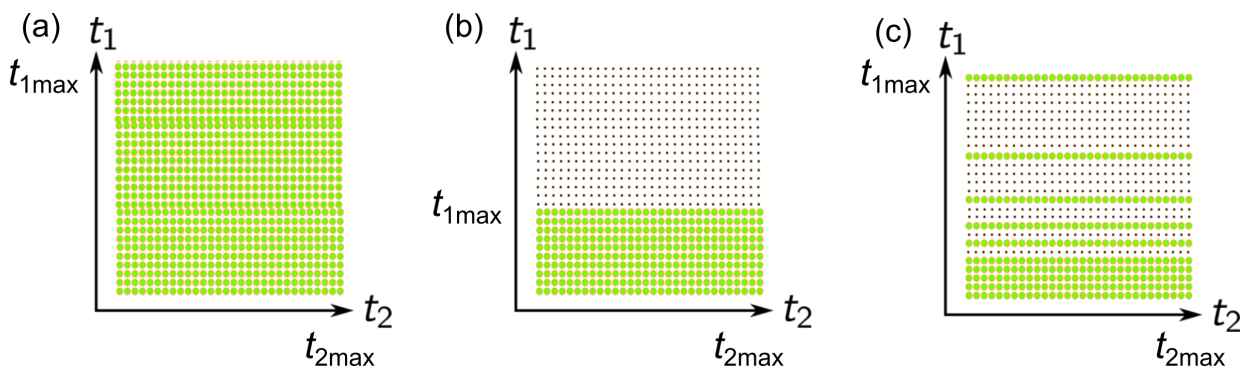


Figure 15.5 Examples of sampling schemes along the indirect evolution period, t_1 , of a 2D NMR experiment: (a) full US, (b) truncated US and (c) exponentially biased random NUS.

NUS data cannot be analyzed using DFT, which requires constant t_1 increment. The analysis of NUS datasets requires the reconstruction of the missing t_1 increments using additional assumptions. Various approaches have been proposed to reconstruct 2D spectra from NUS datasets, including multidimensional decomposition (MDD)⁵⁷, maximum entropy reconstruction,⁵⁸ covariance^{59,60} and compressed sensing (CS).^{61,62} Among these approaches, only the latter two have been experimentally applied for the reconstruction of 2D NMR spectra of oriented media and are discussed in the next subsections. Readers wishing to learn more about the NUS method are invited to read **Chapter 5** in **Part 1** of this book.

15.3.2. Covariance processing

We have demonstrated that covariance can be applied for the reconstruction of symmetric 2D spectra from NUS datasets.⁶³ The number of unknowns for the spectral analysis of NUS datasets is reduced by using the symmetry of the reconstructed 2D spectrum. This covariance processing relies on the fact that two peaks A and B resonating at frequencies, $\nu_{2,A}$ and $\nu_{2,B}$, along direct spectral dimension, F_2 , will exhibit nonzero covariance only if they evolve at the same frequency during t_1 period. This condition holds when two resonances A and B displays diagonal and cross peaks in 2D homonuclear correlation spectra. The covariance spectrum, \mathbf{C} , can be calculated from the 2D mixed time-frequency domain signal, $\mathbf{d} = \text{Re}[s(t_1, \nu_2)]$, as:^{64,65}

$$\mathbf{C} = \left(\frac{1}{N_1(\text{TPPI})} \mathbf{d}^T \cdot \mathbf{d} \right)^{1/2}, \quad (15.9)$$

where \mathbf{d} is acquired using time-proportional phase incrementation (**TPPI**) for quadrature detection along t_1 period with $N_1(\text{TPPI})$ increments in t_1 , and the superscript T denotes the transpose operation. Note here, that the covariance 2D spectrum can also be calculated from datasets acquired using States procedure for quadrature detection along t_1 period.⁶⁵

Covariance reconstruction yields symmetric 2D spectra, in which the indirect dimension is endowed with the same resolution as the direct one. For instance, covariance was applied for the reconstruction of symmetrical 2D ^2H QUOSY spectra, such as the 2D Q-COSY spectrum (see the corresponding pulse sequence in **Figure 15.2a** and the reconstructed spectra in **Figure 15.6b-k**), in which signals exhibit identical resonance frequencies along direct and indirect dimensions.⁶³ Furthermore, NUS allows a further reduction in the number of t_1 increments with respect to truncated US (compare **Figure 15.6h** and **15.6k**). For the sample of **Figure 15.6a**, the combination of NUS and covariance yields a reduction in experimental time by a factor of 2 with respect to truncated US and covariance and by a factor of 5.6 with respect to US and DFT. Furthermore, covariance processing using matrix square root and a suitable regularization method can be employed for quantitative analysis.^{63,66} Hence, 2D NMR spectra

reconstructed using covariance have been employed to measure *ee* and diastereoisomeric excess (*de*) in CLCs.

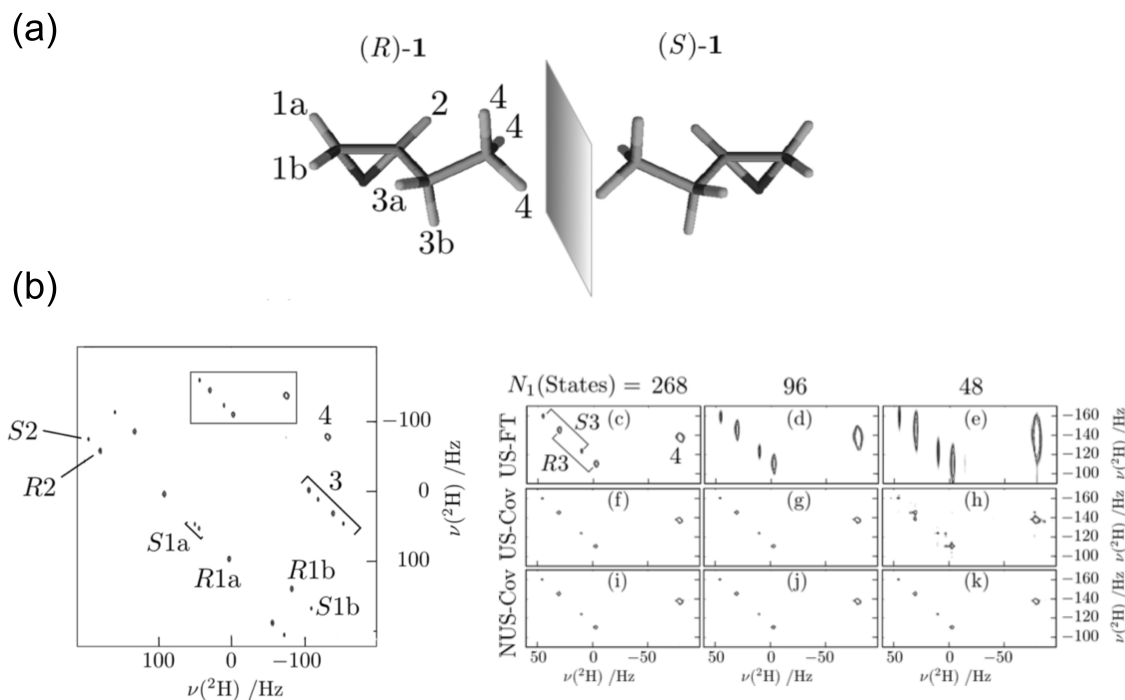


Figure 15.6 (a) Molecular structure of (*R*)- and (*S*)-1,2-epoxybutane (EBT). (b) 92.1 MHz NAD-¹H} Q-COSY Fz US-FT spectrum of EBT with *ee*(*R*) = 50%) recorded in PBLG/CHCl₃ at 300 K with 268 *t*₁ increments. (c) Enlargement of the framed region in spectrum (b). (d-k) Same selected region obtained by different sampling and processing methods: (d,e) DFT-US, (f-h) US-covariance, and (i-k) NUS-covariance. Panels (c,f,i) were processed with 268 *t*₁ increments; panels (d, g, j) were processed with 96 *t*₁ increments; and panels (e, h, k) were processed with 48 *t*₁ increments. For panels (d, e, g, h), the selected data points are those corresponding to the shortest *t*₁ times, whereas for panels (j, k), the data points follow an exponentially decaying distribution. Spectra (f) and (i) are identical because the US and NUS datasets are equivalent when retaining all *t*₁ increments. **Adapted from Ref. 63 with permission from [Wiley].**

15.3.3. Compressed sensing processing

A more general approach for the reconstruction of 2D NMR spectra from NUS datasets is CS.^{67,68,69} This method assumes that the 2D NMR spectrum is sparse, i.e. has few non-zero elements and the sparsest spectrum is the exact one. The sparsest spectrum can be found by the minimization of the norm of the spectrum, subject to the constraint that the reconstructed spectrum is consistent with the measured sample points. This constrained optimization can be converted into an unconstrained optimization by introducing a Lagrange multiplier, λ , and minimizing the objective function:

$$\|i\text{DFT}(\mathbf{f}) - \mathbf{d}\|_{l_2}^2 + \lambda \|\mathbf{f}\|_{l_p}, \quad (15.10)$$

where *i*DFT is the inverse FT operator and $\|\mathbf{X}\|_{l_p}$ is the *l_p*-norm of the vector \mathbf{X} with $p = 2$ for $\mathbf{X} = i\text{DFT}(\mathbf{f}) - \mathbf{d}$ and $0 < p < 1$ for $\mathbf{X} = \mathbf{f}$. The *l_p*-norm of \mathbf{X} vector is defined as:

$$\|\mathbf{X}\|_{l_p} = \left(\sum_{i=1}^N |X_i|^p\right)^{1/p}, \quad (15.11)$$

where N is the number of complex points in the \mathbf{X} vector and X_i is a complex point of \mathbf{X} .

Contrary to covariance, CS can be applied for the reconstruction of asymmetrical 2D NMR spectra from NUS datasets. For instance, CS was employed to reconstruct symmetrical and asymmetrical 2D NAD QUOSY spectra, including Q-COSY and Q-resolved ones (see [Figure 15.7](#)) from NUS datasets.³² Due to the sensitivity enhancement provided by exponentially biased NUS, the combination of NUS and CS results in a four-fold reduction in experimental time with respect to US and DFT without any loss of resolution and sensitivity. Furthermore, the linearity of the integrated intensity was better for NUS and CS than for truncated US and DFT, and hence, spectra reconstructed from NUS datasets using CS allow accurate quantitative measurements, and hence, the determination of ee, for instance.

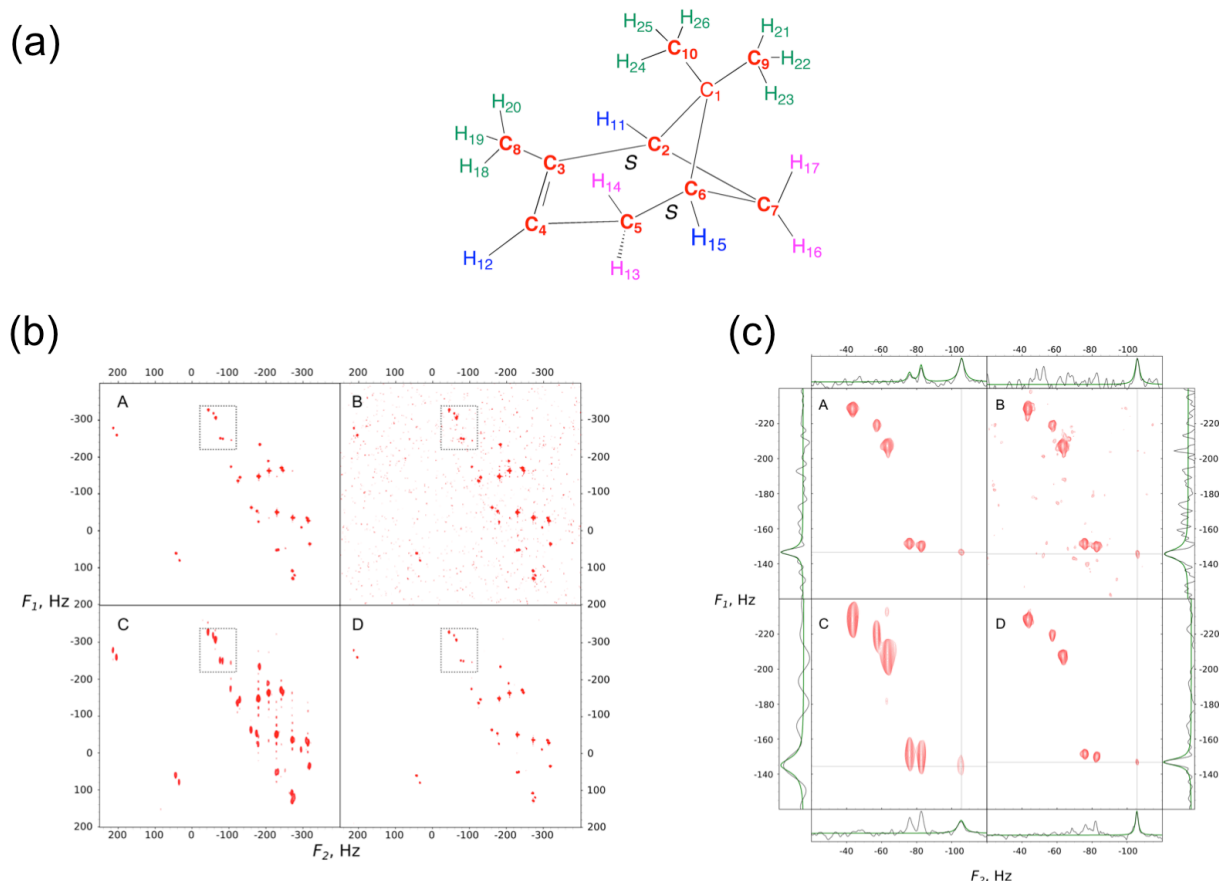


Figure 15.7 (a) Molecular structure of α -pinene. (b) 92.1 MHz NAD Q-resolved F_2 2D spectra of α -pinene enriched in (S,S)-enantiomer and dissolved in PBLG/ CHCl_3 at 300 K acquired with different sampling schedules and reconstructed by different methods: (A) spectrum obtained by FT of US FID with a number of t_1 increments, $N_1 = 256$, and a number of scans, $NS = 64$; (B) spectrum obtained by FT of US FID with $N_1 = 256$ and $NS = 16$; (C) spectrum obtained by FT of US FID with $N_1 = 64$ and $NS = 64$; (D) spectrum obtained by CS reconstruction of NUS FID with $N_1 = 64$ and $NS = 64$. First contour set on eight times the root mean square (rms) noise value (measured in spectrum a). (c) Enlargements of the framed regions in (a). The same labels A-D are used in the panels (a) and (b). **Adapted from Ref. 32 with permission from [RSC].**

15.4. Ultrafast NMR

15.4.1. The spatial encoding based single-scan NMR concept

An important paradigm shift in NMR was the introduction of spatial encoding and UF methods.⁷⁰ These approaches were first developed for isotropic solvents, before being applied to solids and anisotropic media. The principle of UF technique is illustrated in **Figure 15.8b** and is compared to conventional approach proposed by Jeener⁷ for the acquisition of 2D NMR spectra (see **Figure 15.8a**). The principle of UF methods is that spins in different regions of the sample are subject to different t_1 periods.^{51,70,71,72,73,74} Hence, UF methods can be considered as a parallelization of the Jeener approach.

Like in conventional 2D experiments, the spatio-temporal encoding period (k) in UF is preceded by a classical preparation period consisting of a relaxation delay (if a multi-scan experiment is performed) followed by an excitation block. The encoding period combines chirp pulses and gradients to create a spatial encoding of chemical shifts, generally along the z axis. It is followed by a mixing block that transfers coherences to correlate frequencies between indirect and direct dimensions.

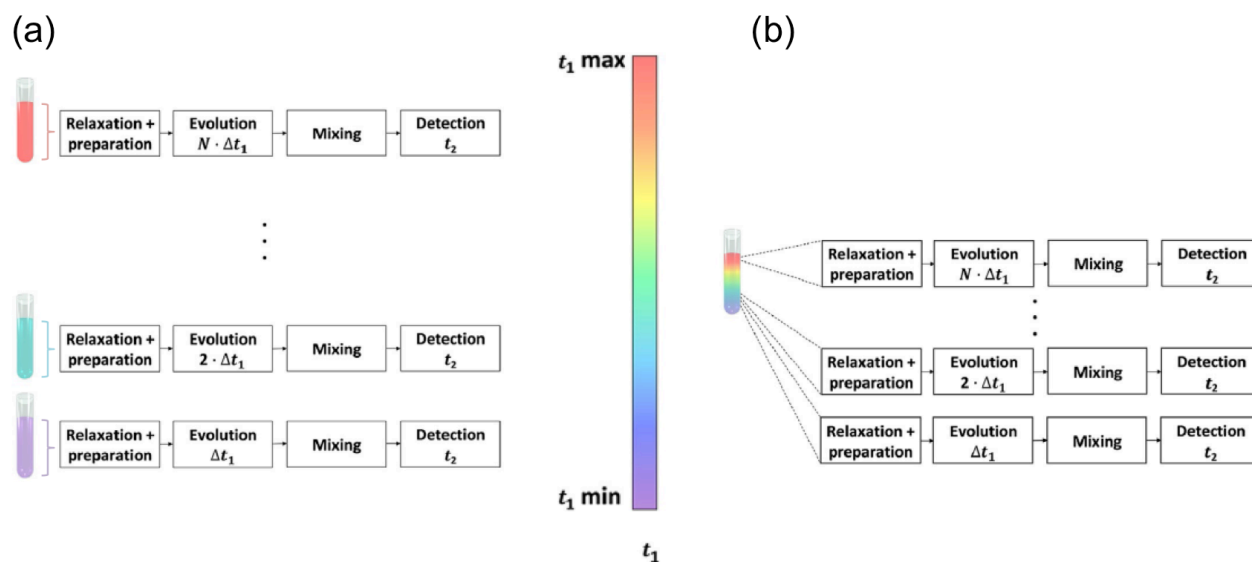


Figure 15.8 General description of Jeener-type (conventional) and UF data acquisition schemes: **(a)** In the approach proposed by Jeener, N_1 experiments are acquired with different t_1 evolution periods. A relaxation delay is necessary between each experiment with t_1 evolution period; **(b)** The UF 2D NMR experiment consists in recording these N_1 experiments on different slices of the sample. **Adapted from Ref. 77 with permission from [Elsevier].**

Finally, the signal is detected in a spatially specific fashion that allows one to distinguish each individual t_1 increment (see [Figure 15.8b](#)) with the help of an oscillating acquisition gradient developed for echo-planar spectroscopic imaging (EPSI) (t_2).^{73,75} After the processing of (k , t_2) raw data, a final spectral map with an UF (k) and conventional (F_2) dimension is obtained. The UF(k) dimension (and subsequently the conventional (F_2) dimension) can be displayed horizontally or vertically on a 2D map depending on the way that data are processed and presented. This approach can be applied for both homo- and heteronuclear nD experiments.^{71,76,77,78} A more detailed description of the UF concept can be found in the [Chapter 7](#) in [Part 1](#) of this book.

15.4.2. Anisotropic $^1\text{H}/^{13}\text{C}$ -HSQC ultrafast NMR

The first UF 2D NMR experiment in anisotropic media was reported in 2013, for ^1H -detected ^{13}C heteronuclear UF 2D sequence in PBLG-based LLCs.⁷⁹ The idea was to propose a fast determination of one bond (^{13}C - ^1H)-RDCs ($^1D_{\text{CH}}$) (accurate and precise data) by recording an 2D ^1H - ^{13}C heteronuclear single quantum coherence (HSQC) spectra⁸⁰ in weakly orienting LLCs in less than a minute.

The 2D sequence proposed for recording single-scan (^1H - ^{13}C)-coupled HSQC 2D spectra is shown in [Figure 15.9](#). This sequence is also suitable for measuring (one bond) ^{13}C - ^1H scalar couplings ($^1J_{\text{CH}}$) in liquids. It can be described as follow: i) after a classical INEPT transfer, the so-called UF dimension of the 2D spectrum is obtained by a multi-echo spatial encoding scheme designed to limit sensitivity losses due to translational diffusion,⁸¹ ii) the evolution of ^{13}C single-quantum coherences under the (one-bond) total ^1H - ^{13}C couplings ($^1T_{\text{CH}} = ^1J_{\text{CH}} + 2^1D_{\text{CH}}$) is refocused during the spatial encoding period, T_e , by applying a 180° ^1H hard pulse in the middle of T_e , iii) the reconversion INEPT block is flanked by two 'folding' gradients capable of arbitrarily shifting resonances in the UF dimension thus reducing the demand on gradient amplitudes,⁸² iv) the signal is finally acquired using an echo-planar-imaging and evolves under $^1T_{\text{HC}}$ as well as ^1H - ^1H total couplings during the acquisition.

This experiment was first demonstrated on a sample of (+)-isopinocampheol ((+)-IPC) dissolved in PBLG-based mesophase using a 500 MHz spectrometer (11.75 T) equipped with 5-mm (o.d.) cryogenic probe as well as a routine gradient unit (50 G/cm). The obtained 2D spectrum processed using the Topspin commercial software and a home-written routine is shown in [Figure 15.9b](#). Compared to conventional coupled HSQC spectrum, the UF HSQC 2D spectrum appears to be rotated by 90° . The $^1T_{\text{CH}}$ values measured on these UF NMR spectra match with those determined from a conventional 2D ω_2 -coupled clean in-phase (CLIP)-HSQC spectrum, recorded in a much longer time.

To the best of our knowledge, no variant of this first UF experiment or other heteronuclear

schemes in combination with oriented solvents has been reported in literature.

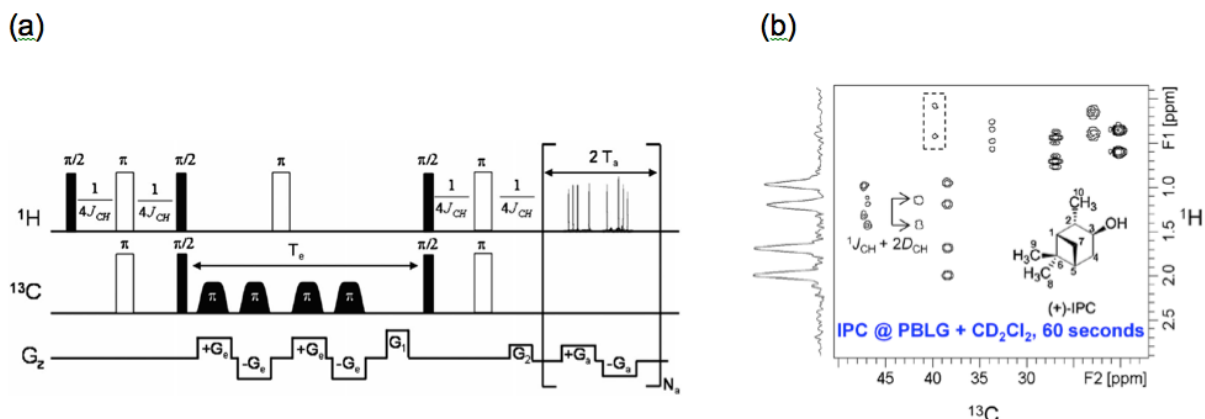


Figure 15.9 (a) Pulse sequence of ultrafast ^1H - ^{13}C -coupled HSQC 2D experiment where G_a and G_e are the acquisition and encoding gradients along z-axis, respectively. The defocusing delays in INEPT transfers are calculated using the average value of $^1J_{\text{CH}}$ or $^1T_{\text{CH}}$ values in isotropic or anisotropic solvents, respectively. (b) (^1H - ^{13}C)-coupled HSQC 2D spectrum of (+)-IPC in PBLG (11.7 T). Details on the experimental conditions can be found in Ref. 79. For the INEPT delays, an average $^1T_{\text{CH}}$ coupling constant of 140 Hz was chosen. Reprinted from Ref. 79 with permission from [Wiley].

15.4.3. Anisotropic ^2H ultrafast NMR (ADUF NMR)

Thanks to many methodological improvements in UF sequences, their performances in isotropic solvents have been notably increased over the last decade, and hence, numerous practical applications has been reported such as quantitative measurements⁸³ including complex biological mixtures,⁸⁴ but also the real-time monitoring of fast chemical transformations (in flow) by NMR using high-field NMR spectrometers^{85,86,87,88} or benchtop NMR equipment (low-field).³⁴

As mentioned above, (C)LCs can be also used as fluid solvents in which chemical reactions/transformations are possible. The results obtained using ^2H NMR in a DNA-based chiral oriented solvent in 2012 have been particularly exciting and led, as we will see below, to the development of ^2H UF 2D NMR sequences for monitoring very fast NMR reactions involving oriented deuterated analytes. As in liquids, the main difficulty of chemical reaction monitoring in real time using ^2H 1D NMR in LCs is the experimental time needed to record NMR data with enough temporal resolution since chemical reactions can proceed in a few minutes or less. These measurements are even more challenging for samples exhibiting numerous ^2H signals corresponding to reactants, intermediates or products since the assignment of ^2H signals in that case does require the acquisition of 2D QUOSY NMR spectra in less than a minute or a few seconds as far as signal-to-noise (S/N) allows.

Clearly, the time reduction provided by NUS methods presented in the previous section is not always sufficient to reach very short experimental times (sub-second). If ASAP 2D experiments can accelerate the acquisition of 2D spectra down to a few dozen of seconds (see **Section**

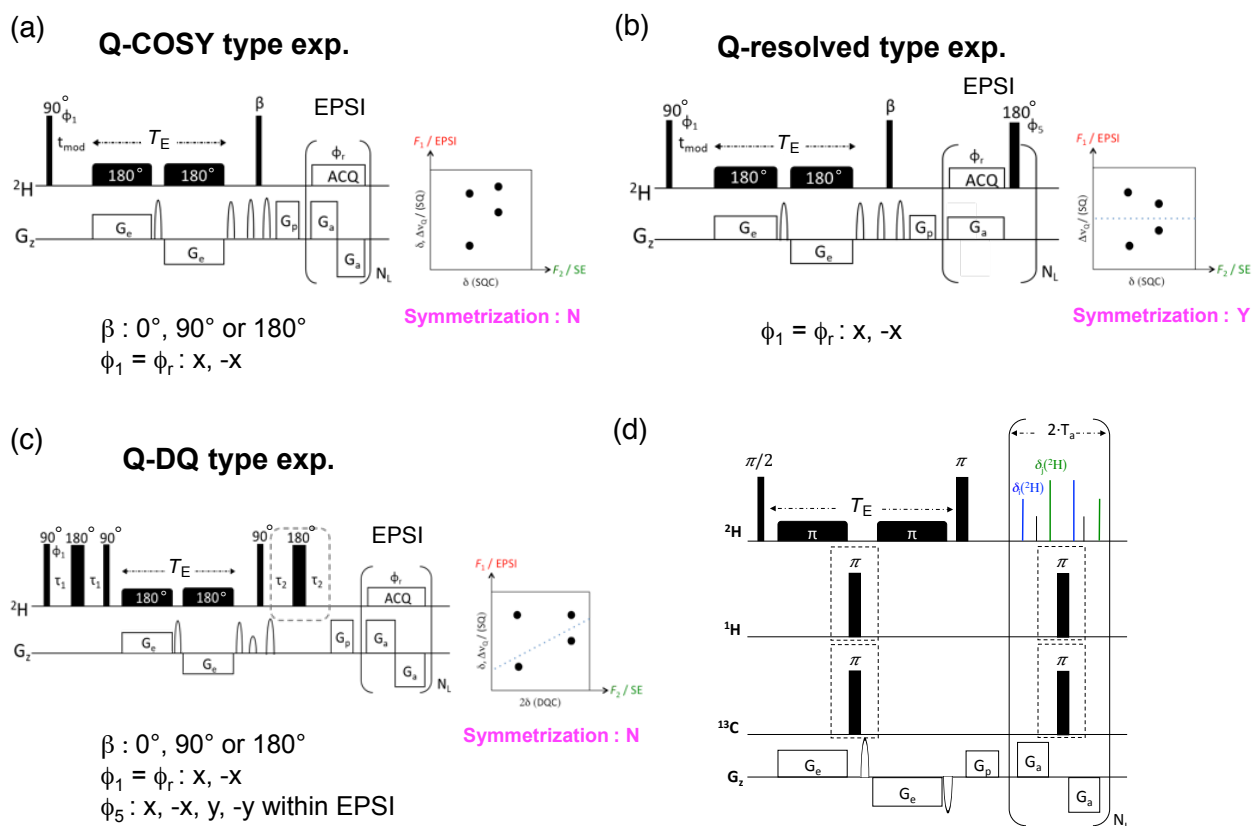


Figure 15.10 (a to c) Basic pulse schemes of Q-COSY, Q-resolved, and Q-DQ 2D ADUF sequences with no ^1H decoupling, and their associated 2D map where the type of coherences (SQC & DQC) is indicated. Here the UF and conventional dimensions are horizontal and vertical, respectively. G_a , G_e and G_p denote the acquisition, encoding and pre-phasing gradients along the z-axis. G_p is used to center the peaks of interest in the middle of the spectral window. N_L denotes the number of loops for EPSI. Horizontal black boxes correspond to ^2H - 180° -chirp pulses. PFG symbolized by a half ellipsoid are for crushing purposes and coherence selection whereas the phase cycling (optional) eliminates possible artifacts when several scans are added. Only the Q-resolved map can be symmetrized. **(d)** A variant of Q-COSY ADUF sequence including two pairs of 180° -hard pulse for both decoupling ^1H and ^{13}C spins (see text). **Adapted from Ref. 30 and 89 with permission from [Wiley] and [RSC].**

15.6), the fastest approach to record 2D experiments consists in the use of UF method, which allows the acquisition of a 2D spectrum in less than a second.

The UF 2D pulse sequence for ^2H nuclei in oriented media was named anisotropic deuterium ultra fast (**ADUF**) experiment and was introduced in 2016 for the acquisition of Q-COSY 2D experiment on a perdeuterated analyte, the *n*-pentanol- d_{12} , dissolved in a PBLG-based chiral mesophase, in less than a second.⁸⁹ The pulse sequence is displayed in **Figure 15.10a/d** and the 2D spectrum recorded at 107.5 MHz (16.5 T) equipped with a TXO cryoprobe is presented in **Figure 15.11a**.

As in case of ^1H UF HSQC, this first ADUF Q-COSY 2D sequence follows a basic scheme where the spatio-temporal encoding, produced by two chirp pulses applied together with a pair of opposite gradients, replaces the usual t_1 evolution time. This block is followed by a conventional mixing period (simpler than in case of HSQC) and a detection block based on

echo planar spectroscopic imaging (**EPSI**). This UF sequence can be analysed using Cartesian spin-operator basis set dedicated for the representation of a single spin-1.³⁰ Relevant operators in a matrix form as well as Hamiltonians are given in Ref. 90.

Disregarding both diffusion and relaxation effects, and without any reading pulses, the resulting echoes (for a single deuterium precession at a frequency, ν) evolve under free-precession leading to the following $S(k, t_2)$ signal:³⁰

$$S(k, t_2) \propto 2i \cos(\pi \Delta \nu_Q TE) \int_{-\frac{L}{2}}^{\frac{L}{2}} \int_0^{t_2} e^{i(k(t_2)z - 2\pi C \nu z)} [e^{i(2\pi \nu + \pi \Delta \nu_Q)t_2} + e^{i(2\pi \nu - \pi \Delta \nu_Q)t_2}] dz dt_2. \quad (15.12)$$

In this equation, TE is the spatial encoding period along the z -axis, L is the length of the sensitive volume of the NMR probe and C is the spatial encoding constant ($C = \frac{4T_c}{L}$ where T_c is the 180° chirp pulses duration) which is similar to the one used for a similar constant time (**CT**) spatial encoding performed on spins-1/2. **Eq. 15.12** indicates that the 2D spectrum exhibits two ^2H 2D-peaks located at $(\nu, \nu + \Delta \nu_Q/2)$ and $(\nu, \nu - \Delta \nu_Q/2)$ after the FT along the t_2 -dimension on the $S(k, t_2)$ map. Although the two ^2H hard-pulses (90_x° pulse followed by a 180_x° pulse) are identical to the conventional Q-COSY sequence leading to magnitude-mode 2D spectra (see **Figure 15.2a**),²² the UF version of Q-COSY scheme is a CT experiment and all type of couplings ($(^2\text{H}-^2\text{H})$ -RDCs and ^2H -RQCs) are refocused along the F_2 dimension. The CT nature of this spatio-temporal encoding is due to the identical time spent in the transverse plane by all spins disregarding their position along the z -axis. Interestingly, the F_2 dimension is therefore a “pure $\delta(^2\text{H})^{\text{aniso}}$ shift” dimension, which simplifies its analysis. Finally note that the associated ^2H - $\{^1\text{H}\}$ UF 2D map is formally identical to that obtained for the conventional ^2H δ -resolved experiments,²¹ except that the spectral content in F_1 and F_2 dimensions are inverted compared to conventional 2D spectra.

Although the spectral resolutions of the ADUF Q-COSY are lower than those of the conventional 2D map (or 1D spectrum),³⁰ the analysis of the ADUF spectrum of [$^2\text{H}_{12}$]-pentan-1-ol (prochiral molecule of C_s -symmetry in average) shows that the discrimination of enantiotopic sites (which is visible for sites 1, 2 and 3) is observed as in case on the conventional 2D spectrum (see **Figure 15.11a**). This loss of resolution in the F_1 dimension of the ADUF spectra is a basic problem originating from the maximum number of loops, N_L , that the gradient amplifier can support in the EPSI block before possible damage. Note here that, the (k, t_2) raw data of UF QUOSY are generally processed with sinusoidal and Gaussian apodization along the conventional and UF dimension.

For non-perdeuterated molecules, a useful variation of the UF Q-COSY sequences is to simply add ^1H - 180° pulses in the middle of the spatial encoding and between successive

acquisition gradients within EPSI to decouple all ^1H spins. Based on the same principle, the decoupling of ^{13}C nuclei can be also performed to eliminate any ^{13}C - ^2H scalar and dipolar coupling observed for ^{13}C -enriched compounds (for instance, see [Figure 15.11d](#)).⁸⁹ This strategy can be applied to any ADUF 2D experiment.

Two other UF ^2H QUOSY experiments were developed in 2020: i) the ADUF Q-resolved experiment that involves only single quantum coherences (**SQC**), and ii) the ADUF Q-DQ experiment that excites the ^2H double-quantum coherence (**DQC**).³⁰ Associated UF sequences and schematic 2D maps are depicted in [Figures 15.10b](#) and [c](#). They can be compared to conventional QUOSY sequences shown in [Figures 15.2](#). In the ADUF Q-resolved sequence, a $\pi(^2\text{H})$ pulse is inserted between two successive reading gradients: $[(G_a) - 180^\circ]_{NL}$ in the EPSI block (see the conventional Q-resolved in [Figure 15.2](#)). This leads to the refocusing of $\delta^{\text{aniso}}(^2\text{H})$, so that the echo amplitudes are now only modulated by $\Delta\nu_Q$, during the t_2 -detection as expressed in [Eq. 15.13](#).³⁰

$$S(k, t_2) \propto 2i \cos(\pi\Delta\nu_Q TE) \int_{-\frac{L}{2}}^{\frac{L}{2}} \int_0^t e^{i(k(t_2)z - 2\pi Cvz)} (e^{i\pi\Delta\nu_Q t_2} + e^{-i\pi\Delta\nu_Q t_2}) dz dt_2 \quad (15.13)$$

Compared to ADUF Q-COSY 2D experiment, the absence of ^2H chemical shifts in the EPSI dimension of Q-resolved is advantageous for two reasons. First, the ^2H signals in the vertical dimension can be symmetrized (no chemical ^2H shift), thus removing artifacts or improving the peak shape. Second, the spectral width provided by EPSI is smaller ($|\Delta\nu_Q^{\text{max}}| \leq SW_{\text{conv}}$) owing to the refocusing of $\delta(^2\text{H})$. As an illustration, [Figure 15.11b](#) shows the ADUF Q-resolved 2D spectrum of [$^2\text{H}_{12}$]-pentan-1-ol (**1**) recorded at 14.1 T in PBLG mesophase where all ^2H -QDs are now symmetrically distributed relative to $F_1 = 0$ Hz.

A ^2H nucleus has a spin $I = 1$, it is therefore possible to excite DQC between energy levels $m_I = +1$ and -1 , which does not evolve under first-order quadrupolar interaction.^{21,30} This “double quantum” ^2H QUOSY 2D experiment is named Quadrupole Double-Quantum (Q-DQ) (see [Figure 15.2c](#)).²¹ The UF version of the ^2H Q-DQ 2D experiment is shown in [Figure 15.10c](#).^{30,91,92}

Considering optimal values of τ_1 and τ_2 equal to $1/(4\Delta\nu_Q)$ and a 90_x° reading pulse, echoes occur during EPSI and can be expressed as:

$$S(k, t_2) \propto \int_{-\frac{L}{2}}^{\frac{L}{2}} \int_0^t e^{i(k(t_2)z - 4\pi Cvz)} \left[e^{i(2\pi\nu + \pi\Delta\nu_Q)t_2} + e^{i(2\pi\nu - \pi\Delta\nu_Q)t_2} \right] dz dt_2. \quad (15.14)$$

As seen on the UF sequence (see **Figure 15-10c**), the preparation period allowing the excitation of the ^2H -DQC is more complex compared to UF Q-COSY or Q-resolved sequences. Theoretically, the amount of ^2H -DQ coherence varies according to the term $\sin(2\pi\Delta\nu_Q\tau_{1,2})$, and

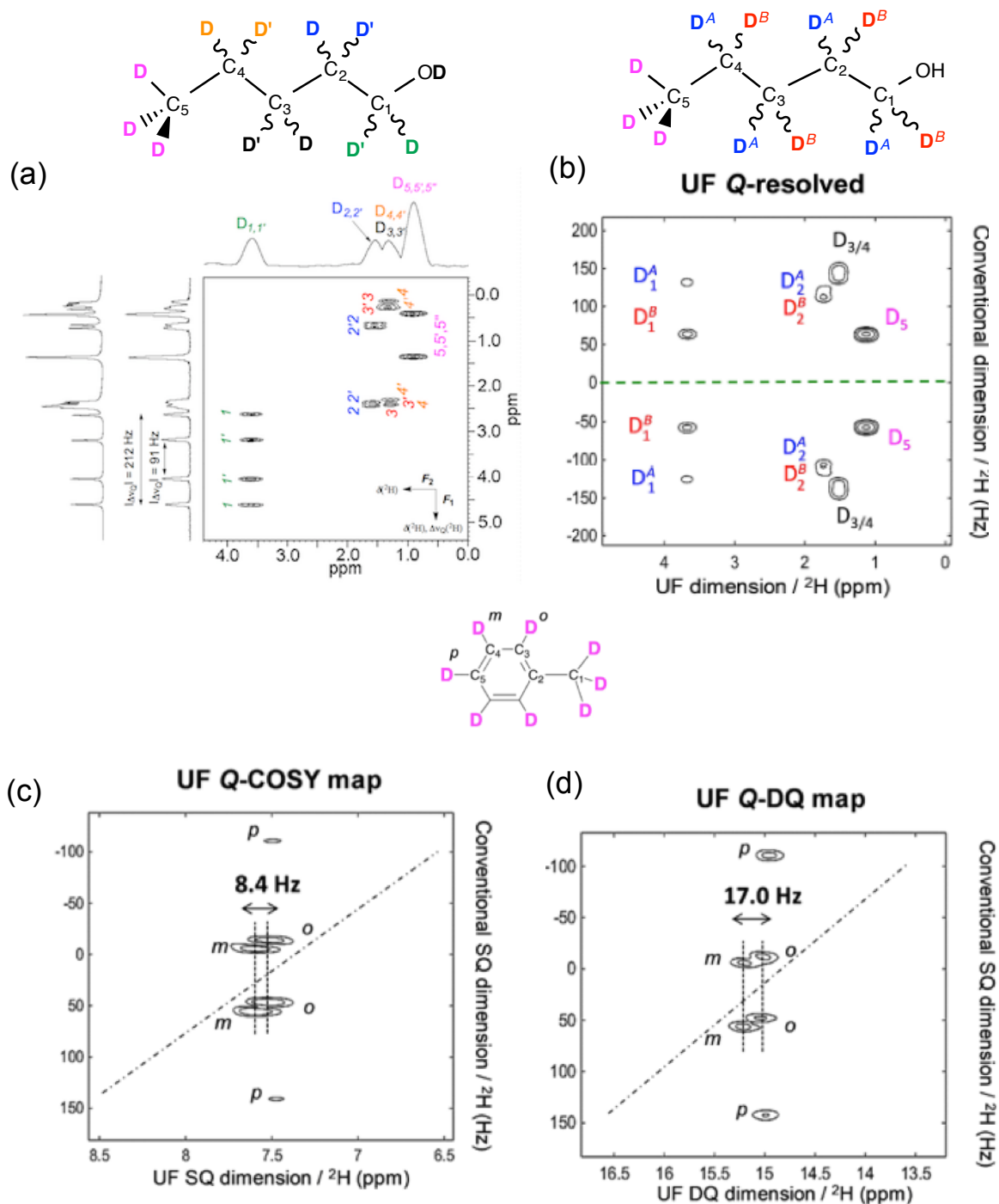


Figure 15.11 (a) 107.5 MHz ADUF- $\{^1\text{H}\}$ Q-COSY 2D map (magnitude mode) of $[\text{H}_{12}]$ -1-pentanol in PBLG/ CHCl_3 ($T_{\text{exp}} = 0.40$ s). In vertical dimension is shown the ^2H - $\{^1\text{H}\}$ 1D spectrum and 2D projection. Note the pair of ^2H -QDs due to spectral discrimination of enantiotopic directions. (b) 92.1 MHz ADUF Q-resolved 2D map of the same sample ($T_{\text{exp}} = 0.20$ s). The pro-*R*/pro-*S* assignment shown by letters *A/B* is arbitrary. (c) Comparison of aromatic regions of 92.1 MHz ADUF Q-COSY and Q-DQ spectra of perdeuterated toluene in PBLG/ CHCl_3 . Both spectra are recorded with a single scan ($T_{\text{exp}} = 0.19$ s). Note the larger spectral separation of ^2H doublets for *meta* and *ortho* positions in the UF dimension of the Q-

DQ spectrum. Experimental details can be found in associated references. **Adapted from Ref. 30 and 89 with permission from [Wiley] and [RSC].**

depends on ^2H -RQCs magnitude associated with each deuterium nucleus. Such a tuning condition does not exist for the two previous sequences. Thereafter, to convert DQC to observable SQC, a reading pulse is applied, potentially followed by a second spin-echo: $90_x^\circ - \tau_2 - 180_x^\circ - \tau_2$ to obtain in-phase signal before detection.

From this equation, we can see, $\delta^{\text{aniso}}(^2\text{H})$'s and ^2H -QD's corresponding to the ^2H -SQC appear in the conventional dimension, while the ^2H -DQC is monitored in the UF dimension leading to echoes occurring at $2\delta^{\text{aniso}}(^2\text{H})$. Thus, each deuterium nucleus gives rise to two 2D-peaks located at $(2\nu, \nu + \Delta\nu_Q/2)$ and $(2\nu, \nu - \Delta\nu_Q/2)$ in frequency units. Sampling $2\delta^{\text{aniso}}(^2\text{H})$ rather than $\delta^{\text{aniso}}(^2\text{H})$ provides an interesting resolution enhancement in the UF dimension for ADUF Q-DQ experiments.

Figure 15.11b and **c** shows a comparison between the ADUF Q-COSY and ADUF Q-DQ 2D spectra (aromatic region) of $[\text{}^2\text{H}_8]$ -toluene in PBLG. As expected, a better resolution of ^2H peaks is observed in the horizontal dimension (UF DQ dimension). This doubling of frequencies can be seen as an analytical advantage for discriminating spectrally close ^2H signals. Reciprocally, this can become an experimental drawback when the molecule presents a large distribution of $\delta^{\text{aniso}}(^2\text{H})$ since a stronger G_a gradient must be applied to reduce the spatial encoding width.

15.4.3.1. ADUF 2D experiments involving another abundant nuclei

Due to its data acquisition mode, the main drawback of UF 2D experiments is related to its low sensitivity. For analytes of reasonable MW ($< 200 - 300 \text{ g.mol}^{-1}$) and/or amounts, the detection of nuclei with high abundance at natural level (as ^1H , ^{19}F , ^{31}P , ...) or after isotopic enrichment (as ^2H , ^{13}C or ^{15}N) is not a problem. Hence, the use of analytes enriched in two isotopes is a possible way to access new additional anisotropic data. For instance, in the absence of any ^{13}C -decoupling (see above), a ^2H - ^{13}C spin-system evolves under $\delta^{\text{aniso}}(^2\text{H})$ and $T(^{13}\text{C}-^2\text{H})$ interactions during spatial encoding of ADUF Q-COSY experiments while $\delta^{\text{aniso}}(^2\text{H})$, $T(^{13}\text{C}-^2\text{H})$ and ^2H -RQC are measured through the EPSI block. For a ^2H - ^{13}C pair, four 2D-peaks are observed at the frequency positions given in **Table 15-3**.

Table 15-3. Location in frequency units of the 2D-peaks pertained to ADUF Q-COSY 2D experiment applied on a ^2H - ^{13}C spin-system³⁰

| UF dimension (Hz) | Conventional dimension (Hz) ^a |
|--|--|
| $\nu^{\text{aniso}}(^2\text{H}) + T(^{13}\text{C}-^2\text{H})/2$ | $\nu^{\text{aniso}}(^2\text{H}) + [T(^{13}\text{C}-^2\text{H}) + \Delta\nu_Q(^2\text{H})]/2$ |
| $\nu^{\text{aniso}}(^2\text{H}) + T(^{13}\text{C}-^2\text{H})/2$ | $\nu^{\text{aniso}}(^2\text{H}) + [T(^{13}\text{C}-^2\text{H}) - \Delta\nu_Q(^2\text{H})]/2$ |

$$\begin{array}{ll} \nu^{\text{aniso}}(^2\text{H}) - T(^{13}\text{C}-^2\text{H})/2 & \nu^{\text{aniso}}(^2\text{H}) - [T(^{13}\text{C}-^2\text{H}) + \Delta\nu_{\text{Q}}(^2\text{H})]/2 \\ \nu^{\text{aniso}}(^2\text{H}) - T(^{13}\text{C}-^2\text{H})/2 & \nu^{\text{aniso}}(^2\text{H}) - [T(^{13}\text{C}-^2\text{H}) - \Delta\nu_{\text{Q}}(^2\text{H})]/2 \end{array}$$

For illustration, **Figure 15.12** shows the ADUF Q-COSY map of benzyl alcohol enriched in both ^2H and ^{13}C isotopes on the methylene group and dissolved in a PBLG mesophase. In this example, the two enantiotopic heteronuclear directions, $(^{13}\text{C}-^2\text{H}^{\text{A}})$ and $(^{13}\text{C}-^2\text{H}^{\text{B}})$, exhibit inequivalent patterns as described in **Table 15-3**, but with different coupling constants, e.g. $\Delta\nu_{\text{Q}}(^2\text{H}^{\text{A}}) \neq \Delta\nu_{\text{Q}}(^2\text{H}^{\text{B}})$ and $|T(^{13}\text{C}-^2\text{H}^{\text{A}})| \neq |T(^{13}\text{C}-^2\text{H}^{\text{B}})|$.

Projections along the conventional dimension enable unambiguous measurements of the spin-spin total couplings, $|T(^{13}\text{C}-^2\text{H}^{\text{A/B}})|$ and $\Delta\nu_{\text{Q}}(^2\text{H}^{\text{A/B}})$. Interestingly, if the experiment is carried out with a sufficient number of loops for the EPSI block, it becomes possible to reach a sufficient resolution (here nearby 3 Hz) to probe the ^2H -homonuclear total couplings: $|T(^2\text{H}^{\text{A}}-^2\text{H}^{\text{B}})|$. *De facto*, we can extract another order-dependent parameter, and hence such experiments make accessible three anisotropic parameters that might be useful for specific analysis.

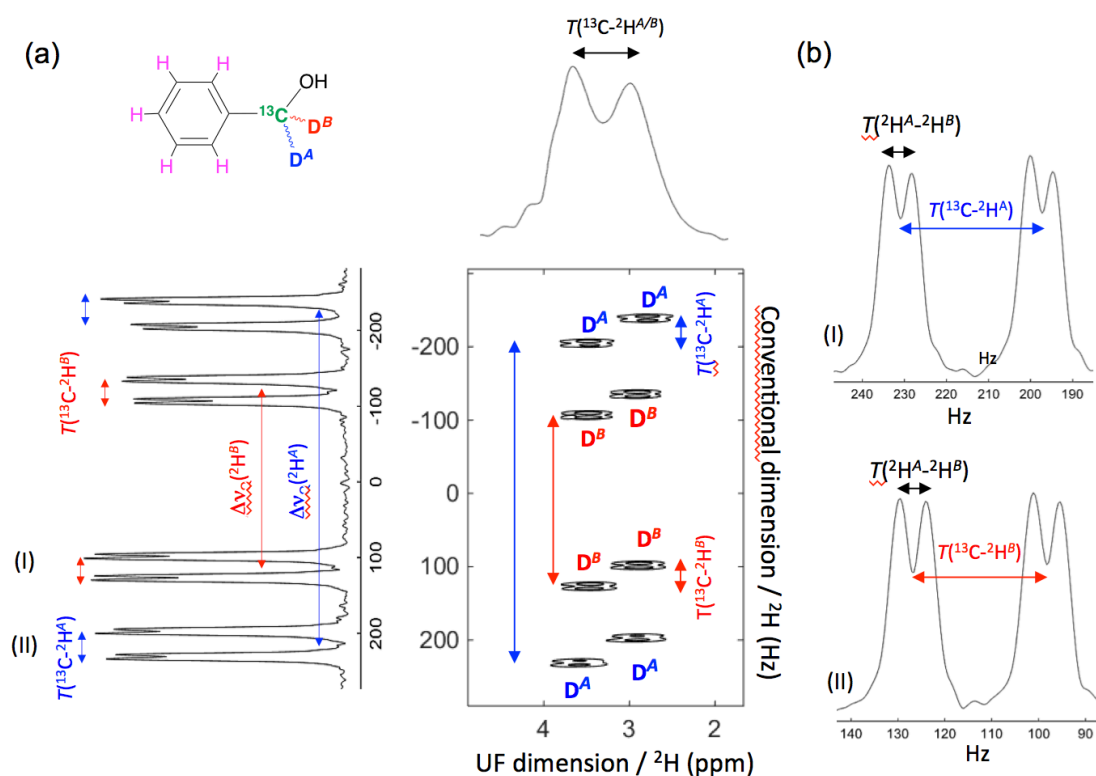


Figure 15.12 (a) 92.1 MHz ADUF- $\{^1\text{H}\}$ Q-COSY 2D spectrum of ^2H , ^{13}C -labelled benzyl alcohol in PBLG/ CHCl_3 ($T_{\text{exp}} = 0.365$ s), with $T_{\text{E}} = 60$ ms and EPSI block of $N_{\text{L}} = 256$ pairs of alternative gradients. The sum-projections along both dimensions are shown. The vertical projection enables an accurate measurement of $|\Delta\nu_{\text{Q}}(^2\text{H}^{\text{A}})| = 436$ Hz and $|\Delta\nu_{\text{Q}}(^2\text{H}^{\text{B}})| = 234$ Hz. (b) Zoomed regions allowing a clear measurement of $|T(^{13}\text{C}-^2\text{H}^{\text{A}})| = 34$ Hz, $|T(^{13}\text{C}-^2\text{H}^{\text{B}})| = 29$ Hz and $|T(^2\text{H}^{\text{A}}-^2\text{H}^{\text{B}})| = 5$ Hz. The stereodescriptors

A and *B* are arbitrarily defined. Experimental details can be found in Ref. 30. Adapted from Ref. 30 with permission from [Wiley].

15.4.3.2. ADUF 2D experiments at natural abundance level (ANADUF)

Compared to any conventional 2D experiments, ADUF experiments suffer from a lack of sensitivity originating from the single-scan 2D experiment principle, itself. This effect can be very critical for nuclei with low natural abundance or low gyromagnetic ratio as in case of ^2H nuclei at natural abundance. In 2020, it has been, however, demonstrated that ADUF experiments could be recorded on isotopically unmodified analytes, and not only on isotopically enriched analytes.³⁰ This experiment is known as **ANADUF** (Anisotropic Natural Abundance Deuterium Ultrafast). As the total couplings, $T(^2\text{H}-^2\text{H})$, are rarely observed in isotopically enriched molecules dissolved in weakly aligning media (very small magnitudes) and never detected at NAD level (too low probability of detecting dideuterated isotopomers), the complexity of $^2\text{H}\{-^1\text{H}\}$ 1D/2D spectra of enriched (perdeuterated) and isotopically normal solutes are identical, except that the intensity of NAD signals is divided by a factor of 6451.³⁰

The possibility of recording ANADUF 2D experiments of oriented solutes appear highly challenging for three reasons: i) the anisotropic signal of ^2H nuclei is divided into two components in a LC and potentially four components in a CLC, if one considers the case of spectrally discriminated enantiomers or enantiotopic directions, ii) ANAD lines can be broadened along the spatial encoding dimension when the aligned sample is not perfectly homogeneous or does not exhibit uniform orientation, and iii) the $T_2^{\text{aniso}}(^2\text{H})$ are generally shorter than $T_2^{\text{iso}}(^2\text{H})$. However the evaluation of the potential of ADUF experiments under extreme conditions of low sensitivity cannot be simply considered as an academic challenge, given the sensitivity gains provided by the new generation of high-field NMR spectrometers equipped with a selective ^2H cryogenic probe and hyperpolarization techniques, for which single-scan 2D acquisition is the best suited option.^{40,41,42}

The first ever 2D ANADUF- $\{^1\text{H}\}$ experiment used an achiral compound of C_{2v} -symmetry in average, the 2,3,6-trimethylphenol dissolved in the PBLG/ CH_2Cl_2 phase. The choice of this analyte was governed by its large numbers of equivalent ^2H sites (two chemically equivalent methyl group, another methyl group and two equivalent methine groups) with relative populations of $P = 6 : 3 : 2$. To reach exploitable ANADUF spectra with sufficient sensitivity, it was however necessary to add 58 scans, *i.e.* an experimental time, T_{exp} , of 120 s (with $T_{\text{R}} = 2$ s) (see **Figure 15.13**). If this ANADUF 2D first spectrum validates the proof of concept, its analytical content remains rather poor since only the NAD-QDs of the pair of equivalent methyl groups ($P = 6$) and dichloromethane emerge from the spectral noise, contrarily to the conventional anisotropic NAD- $\{^1\text{H}\}$ Q-COSY 2D spectrum.

From this example, it could be possible to further maximize the intensity of ANADUF- $\{^1\text{H}\}$ signals by optimizing the NMR sample and/or experimental parameters, according to the [Eq. 15.15](#).³⁰

$$[{}^2\text{H}_i] = \left(\frac{k \times V_{\text{coil}}}{V_{\text{sample}}} \right) \times \left(\frac{m_A}{M_A} \right) \times P_i \times \left(\frac{{}^2\text{H}}{{}^1\text{H}} \right)_i. \quad (15.15)$$

In this equation, k is the response factor of the coil and V_{coil} is the efficient volume of the probe (evaluated at 18 mm³) and $({}^2\text{H}/{}^1\text{H})$ is the isotopic ratio at site i . Thus, it can be envisaged to increase the concentration in monodeuterated isotopomers by increasing the solute mass, while reducing the organic co-solvent volume of sample.

From a more NMR perspective, we can increase the number of scans and/or reduce the recycling time of the experiments. However, a too short T_{R} delay combined with too many scans could possibly damage the gradient coil of the cryogenic NMR probe, while the concept of UF experiments may appear as rather usurped for T_{exp} around a ten of minutes.

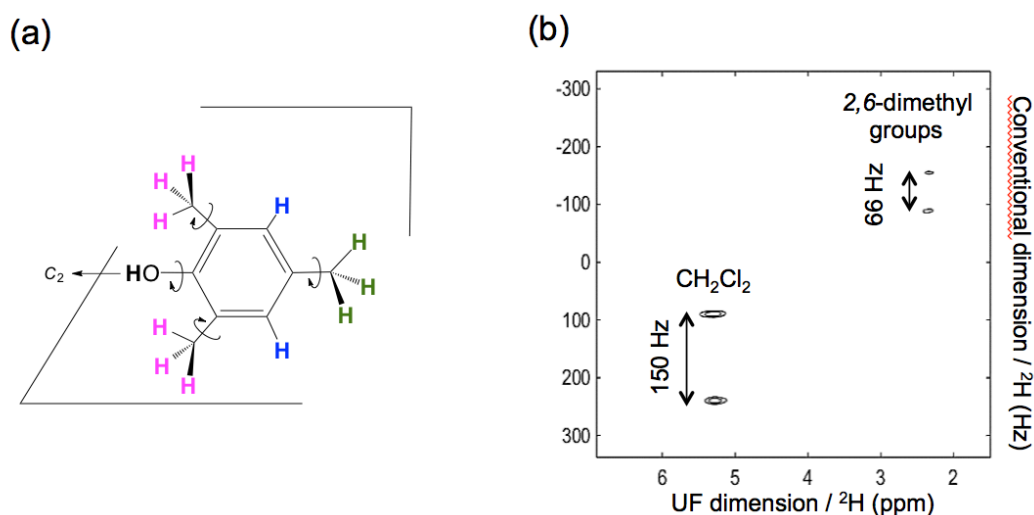


Figure 15.13 First example of ANADUF- $\{^1\text{H}\}$ Q-COSY 2D spectrum (92.1 MHz) recorded in 120 s using the 2,4,6-trimethylphenol as test compound. The ${}^1\text{H}$ decoupling is ensured by a simple 180° hard pulse, both in the middle of the EPSI and UF dimension of the sequence. 58 scans with a recycling delay of 2 s have been averaged to reach a SNR equal to 48 and 23 for the NAD signal of co-solvent (CH_2Cl_2) and the in *ortho*-position methyl groups of analyte, respectively. **Reprinted from Ref. 30 with permission from [Wiley].**

15.5. ASAP NMR

In previous sections, we have described how NUS and UF techniques can accelerate the acquisition of anisotropic 2D NMR spectra, mainly of ${}^2\text{H}$ isotope. These two approaches result in very distinct ranges of overall experimental times (tens of minutes for NUS, instead of sub-second for UF). A third approach, which has been applied for the rapid acquisition of 2D spectra

in oriented, is the fast pulsing technique for enhancing the sensitivity. This strategy allows recording 2D ^1H - ^{13}C heteronuclear correlation spectra and the measurement of $^1T_{\text{CH}}$ couplings within tens of seconds.^{17,93} In particular, the concepts of “alternate SOFAST” (ALSOFAST) and “acceleration by sharing adjacent polarization” (ASAP) were applied to acquire (^{13}C - ^1H) HSQC-type 2D schemes (CLIP/CLAP-HSQC for instance).^{17,93,94,95}

In **Figure 15.14a** is depicted the pulse sequence ^1H , ^{13}C -ASAP-HSQC 2D experiment combining the ASAP approach and the CLIP-HSQC sequence, which allows the acquisition of the clean in-phase ^{13}C - ^1H heteronuclear coupled doublets. The ASAP HSQC sequences detect the protons covalently bound to ^{13}C nuclei, whereas the magnetization of the other protons is stored along the direction of the B_0 field before the application of the pulsed field gradients and is employed as a polarization reservoir for the following scan. Between consecutive scans, a mixing sequence lasting typically 25–40 ms distributes the magnetization over all protons, including those bound to ^{13}C nuclei.^{17,95} The defocusing delay of HSQC sequence is optimized according to the Ernst angle approach to minimize the delay between scans. The variant without mixing is called ALSOFAST-HMQC and is notably beneficial for molecules exhibiting rapid transverse relaxation.⁹⁶ A detailed description of this concept and the ASAP- and ALSOFAST-HSQC experiments can be found in **Chapter 3** of this book.

As illustrating example, **Figure 15.14b** shows the ω_2 -coupled CLIP-ALSOFAST-HSQC spectrum recorded in about 25 s overall experiment time, in the case of sucrose in a partially aligned PEO/ D_2O -based gel. As seen on this example, this combined approach allows an accurate extraction of one-bond (^1H - ^{13}C)-RDC data in partially aligned samples (and $^1J_{\text{CH}}$ in isotropic samples) in less than half a minute, the overall experimental time depending mainly on

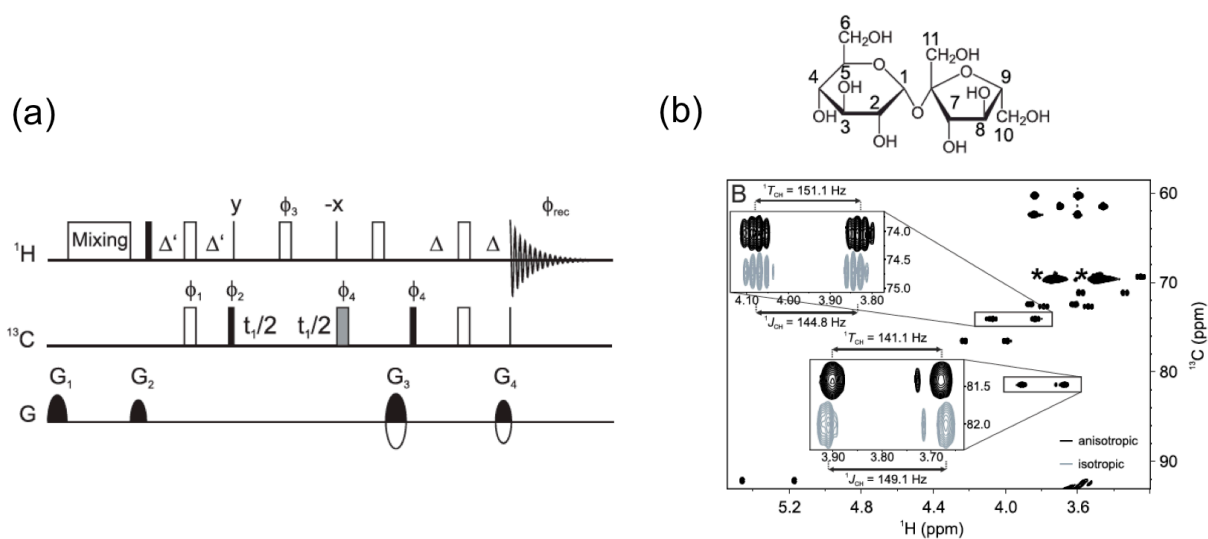


Figure 15.14 (a) Pulse sequence of the ^1H , ^{13}C -CLIP-ASAP-HSQC experiment. Thin and thick vertical lines correspond in all cases to 90° pulses, details on the type of shaped pulses and shaped pulse sandwiches (thick line and black boxes) can be found in Ref. 17. Pulse phases are x unless indicated otherwise. **(b)** ω_2 -coupled CLIP-ALSOFAST-HSQC spectrum of sucrose in a partially aligned 100mM

sucrose sample in PEO/D₂O obtained in 25 s overall experiment time with the use of the CLIP-ALSOFAST-HSQC pulse sequence. Zooms of the signals 8 and 9 show the comparison of ¹³C-¹H doublets in this isotropic sample with those measured in an isotropic solvent (D₂O). **Adapted from Ref. 17 with permission from [Wiley].**

the number of t_1 -increments chosen accordingly to the ¹³C chemical shift dispersion of the molecule. Further variants of the CLIP-ASAP/ALSOFAST-HMQC sequence were also developed, notably to minimize the artifact intensities.⁹³ Moreover, additional reduction in experimental time was achieved by combining this fast pulsing technique with NUS. This possibility was notably demonstrated for partially aligned sucrose molecules in a stretched PEODA/D₂O gel.⁹³

15.6. From anisotropic media to solid-state NMR

Principles of fast NMR, first tested in liquids, have also been extended to solid-state NMR under magic-angle spinning (**MAS**). As no specific chapter is devoted to this subject in this book, and even if it is beyond the scope of this chapter, we will just briefly mention some recent advances in that field.

The fast acquisition of multidimensional NMR spectra can be more challenging for solids than for isotropic solutions or oriented media since NMR resonances of solids are generally broader than those of solutions and hence, the NMR spectra of the former are less sparse and less sensitive.

Nevertheless, the usefulness of NUS approaches was demonstrated for the acquisition of multidimensional NMR spectra, which were reconstructed using various techniques, including MDD⁹⁷, covariance,⁹⁸ maximum entropy,⁹⁹ CS,¹⁰⁰ and iterative algorithms, which remove the point-spread function artefacts.¹⁰¹ NUS was applied for the acquisition of various multidimensional NMR spectra of solids, including 2D and 3D homo- and hetero-nuclear spectra of biological solids, including proteins and viruses,^{97,98,99,100,101,102} but also more recently for 2D heteronuclear correlation between spin-1/2 and quadrupolar nuclei in inorganic materials.^{103,104}

Non-Jeener methods, including frequency-domain sampling combined with Hadamard transform as well as spatial or orientational encoding, were also applied for the fast acquisition of 2D spectra of solids. Frequency-domain sampling consists in exciting selectively the frequency-regions containing signals using frequency-selective pulses.⁵² The frequency is optimized by exciting simultaneously different regions using an array of pulses exciting different frequencies with phases varied in different scans according to the Hadamard matrix so that the signals corresponding to the different frequency regions can be retrieved using Hadamard transform. Hadamard spectroscopy can significantly reduce the experimental time when the number of signals is limited and the spectral width is large. This technique has notably been employed for the fast acquisition of 2D ¹³C-¹³C and ¹³C-¹⁵N correlation spectra.^{105,106,107}

UF NMR has also been employed to accelerate the acquisition of 2D ^1H homocorrelation NMR spectra of semisolids and natural rubber.^{108,109,110} These experiments, however, require a MAS probe equipped with gradient coils or a magnet equipped with microimaging device. These types of instruments are not widely available today. Furthermore, UF NMR is mainly useful for soft solids exhibiting long transverse relaxation times, whereas for hard solids, the coherence lifetime can be shorter than the length of the pulsed field gradient. Note that another variant of UF NMR has been proposed for solids under MAS conditions. The spatial encoding by the pulsed field gradients is replaced by orientational encoding, *i.e.* the crystallites with different orientations are subjected to distinct indirect evolution periods, t_1 .¹¹¹ Nevertheless, the implementation of orientational encoding is challenging because it requires frequency-selective pulses, which are much shorter than the rotor period. This condition is especially difficult to fulfill at high MAS frequencies.

15.7. Overview and prospects

In this Chapter, we have described how NUS, fast pulsing and UF techniques can reduce the experimental time of 2D NMR spectra in anisotropic media down tens of minutes, tens of seconds, and sub-second, respectively. NUS reduces the overall experimental time typically by a factor of 2 to 4, when the duration of the experiment is limited by the sampling along the indirect evolution period, t_1 . Furthermore, by matching the sampling density and the signal envelope, NUS also yields sensitivity enhancements, which can be useful for the detection of diluted isotopes, such as ^2H in isotopically unmodified analytes. Conversely, UF NMR allows the rapid acquisition of 2D NMR spectra in anisotropic media for isotopes of high natural abundance or for isotopically enriched samples. These UF NMR experiments are expected to be useful to monitor very fast chemical reactions in oriented media and notably to observe stereochemical changes, such as racemization, which cannot be observed in isotropic solution. Finally, fast pulsing approaches enhancing polarisation, such as ASAP and ALSOFAST, can be used to accelerate the acquisition of ^1H , ^{13}C -HSQC-type experiments and the measurements of (^1H - ^{13}C)-RDCs, which may provide precious structural information.^{5,6} These fast pulsing approaches can be combined with NUS but cannot be applied for the acquisition of ^2H NMR spectra owing to the small ^2H - ^1H total spin couplings.

Furthermore, with the developments of NMR magnets with ^1H Larmor frequency higher than 1 GHz and hyperpolarization techniques, such as DNP, which boosts the sensitivity of NMR experiments, the duration of NMR experiments will be more often limited by the sampling along the indirect dimension rather by the sensitivity, hence, increasing the application range of fast 2D NMR in anisotropic media.

Acknowledgements

The authors thank all local, national, international scientific partners and colleagues who successfully contributed to the methodological developments described in this Chapter and beyond. P.L. acknowledges CNRS and the Université Paris-Saclay (formely Université Paris-Sud) for their recurrent funding of fundamental research. O.L. thanks the Chevreul Institute (Grant No. FR 2638), Ministère de l'Enseignement Supérieur, de la Recherche et de l'Innovation, Hauts-de-France Région and FEDER for supporting and partially funding this work.

Abbreviations

| | |
|---------------------------|--|
| ADUF: | Anisotropic deuterium ultrafast |
| AR: | Alanine racemase |
| ALC: | Achiral liquid crystal |
| ALSOFAST: | Alternate SOFAST |
| ANAD: | Anisotropic natural abundance deuterium |
| ANADUF: | Anisotropic natural abundance deuterium ultrafast |
| ASAP: | Acceleration by sharing adjacent polarization |
| Cov: | Covariance transformation |
| CLC: | Chiral liquid crystal |
| CPD: | Composite pulse decoupling |
| CS: | Compressed sensing |
| CT: | Constant time |
| DNP: | Dynamic nuclear polarization |
| DQC: | Double-quantum coherence |
| DE (<i>de</i>): | Diastereomeric excess |
| EE (<i>ee</i>): | Enantiomeric excess |
| EFG: | Electric field gradient |
| EPSI: | Echo-planar spectroscopic imaging |
| FID: | Free induction decay |
| FT: | Fourier transformation |
| FWHM: | Full width at half maximum |
| HETCOR: | Heteronuclear correlation |
| HSQC: | Heteronuclear single quantum coherence |
| INADEQUATE: | Incredible natural abundance DQ transfer experiment |
| LC: | Liquid crystal |
| LLC: | Lyotropic liquid crystal |
| MAS: | Magic-angle spinning |
| <i>n</i>D NMR: | Multidimensional NMR ($n = 2, 3 \dots$) |
| NAD: | Natural abundance deuterium |
| NAD-¹H: | Natural abundance deuterium with ¹ H decoupling |
| NMR: | Nuclear magnetic resonance |
| NUS: | Non-uniform sampling |
| PBLG: | Poly- γ -benzyl- <i>L</i> -glutamate |
| PFG: | Pulsed field gradient |
| Q-COSY: | Quadrupolar correlation spectroscopy |
| Q-COSY Fz: | Quadrupolar correlation spectroscopy with z-gradient filter |
| QD: | Quadrupolar doublet |
| Q-DQ: | Quadrupolar double-quantum |
| QUOSY: | Quadrupole ordered spectroscopy |
| Q-resolved: | Quadrupolar resolved experiment |
| Q-resol. Fz: | Quadrupolar resolved experiment with z-gradient filter |
| RCSA: | Residual chemical shift anisotropy (noted also σ_i^{aniso}) |
| RDC: | Residual dipolar coupling (noted also D_{ij}) |
| R-NASDAC: | Refocussed natural abundance spectroscopy for deuterium and carbon |
| RQC: | Residual quadrupolar coupling (noted also $\Delta\nu_{Qj}$) |
| SNR: | Signal-to-noise ratio |
| SQC: | Single-quantum coherence |

| | |
|----------------|--|
| SS-NMR: | Solid-state NMR |
| TPPI: | Time-proportional phase incrementation |
| UF: | Ultrafast |
| US: | Uniform sampling |

NMR notations or greek symbols used

| | |
|---------------------|---|
| B_0 : | Static magnetic field produced by NMR magnet |
| D_{ij} : | Residual dipolar coupling between nuclei i and j |
| $\Delta \nu_{Qi}$: | Quadrupolar splitting of nucleus i (spin $I > 1/2$) |
| G_a : | Acquisition gradient |
| G_e : | Encoding gradient |
| G_p : | Pre-phasing gradients |
| γ_i : | Gyromagnetic ratio of nucleus i |
| J_{ij} : | Scalar coupling between nuclei i and j |
| K_{C-D} : | ^2H -quadrupolar coupling constant |
| N_a or N_L : | Loop number (EPSI acquisition block) |
| Q_{Di} : | Nuclear electric quadrupolar moment of nucleus i |
| r_{ij} : | Internuclear vector between nuclei i and j |
| $S_{\alpha\beta}$: | Saupe order matrix |
| S_{ij} : | Local internuclear orientational order of i-j internuclear vector |
| T_A or T_a : | Acquisition time |
| T_E or T_e : | Spatial encoding duration |
| T_{exp} : | Experimental time |
| T_{ij} : | Total spin-spin coupling between nuclei i and j |
| T_R : | Recycling delay |
| t_1 : | Indirect evolution period |
| t_2 : | Acquisition period |
| T_1 : | Longitudinal relaxation time |
| T_2 : | Transverse relaxation time |
| V_{C-D} : | Electric field gradient (along a C-D bond) |

References

1. J.W. Emsley and J. Feeney, *Prog. Nucl. Magn. Reson. Spectrosc.*, 1995, **2**, 1.
2. B. Reif, S.E. Ashbrook, L. Emsley and M. Hong, *Nat. Rev. Methods Primers*, 2021, **1:2**, 1.
3. P. Giraudeau, *Analyst*, 2020, **145**, 2457.
4. S.C. Chiliveri, A.J. Robertson, Y. Shen, D.A. Torchia and A. Bax, *Chem. Rev.*, 2022, **122**, 9307.
5. P. Lesot, C. Aroulanda, P. Berdagué, A. Meddour, D. Merlet, J. Farjon, N. Giraud and O. Lafon, *Prog. Nucl. Magn. Reson. Spectrosc.*, 2020, **116**, 85.
6. C. Aroulanda and P. Lesot, *Chirality*, 2022, **34**, 182.
7. J. Jeener, Lecture notes from Ampere Summer School in Basko Polje, Yugoslavia, September, 1971, later reprinted in *NMR and More in Honour of Anatole Abragam*, Eds. M. Goldman and M. Porneuf, Les Éditions de Physique, Avenue du Hoggar, Zone Industrielle de Courtaboeuf, France (1994).
8. W.P. Aue, E. Bartholdi and R.R. Ernst, *J. Chem. Phys.*, 1976, **64**, 2229.
9. R.R. Ernst and W.A. Anderson, *Rev. Sci. Inst.*, 1966, **37**, 93.
10. J.W. Emsley and J.C. Lindon, (Eds.) in book: *NMR Spectroscopy Using Liquid Crystal Solvents*, Pergamon Press, Oxford. Chap. 2, (1975).
11. R.R. Gil, C. Gayathri, N.V. Tsarevsky and K. Matyjaszewski, *J. Org. Chem.*, 2008, **73**, 840.
12. J.C. Freudenberger, P. Spiteller, R. Bauer, H. Kessler and B. Luy, *J. Am. Chem. Soc.*, **2004**, **126**, 14690.
13. M. Sarfati, P. Lesot, D. Merlet and J. Courtieu *Chem. Commun.*, 2000, 2069.
14. J. Farjon, D. Merlet, P. Lesot and J. Courtieu, *J. Magn. Reson.*, 2002, **158**, 169.
15. J. Farjon, J.-P. Baltaze, P. Lesot, D. Merlet and J. Courtieu, *Magn. Res. Chem.*, 2004, **42**, 594.
16. J. Farjon and N. Giraud, *Current Opinion in Colloid & Interface Science*, 2018, **53**, 1.
17. J. Becker and B. Luy, *Magn. Reson. Chem.* 2015, **53**, 878.
18. T. Reinsperger and B. Luy, *J. Magn. Reson.*, 2014, **239**, 110.
19. P. Trigo-Mouriño, A. Navarro-Vazquez, J. Ying, R.R. Gil and A. Bax, *Angew. Chem., Int. Ed.*, 2011, **50**, 7576.
20. R.R. Gil, C. Griesinger, A. Navarro-Vazquez and H. Sun, Structural elucidation of small organic molecules assisted by NMR in aligned media. (2014). Edited by Cid, Maria-Magdalena; Bravo, Jorge. From *Structure Elucidation in Organic Chemistry*, 279-323. Wiley-VCH Verlag GmbH & Co. KGaA. Weinheim, Germany. ISBN: 978-3-527-66461-0, DOI: 10.1002/9783527664610.ch8.
21. D. Merlet, B. Ancian, J. Courtieu and P. Lesot, *J. Am. Chem. Soc.*, 1999, **121**, 5249-5258.
22. O. Lafon, P. Lesot, D. Merlet and J. Courtieu. *J. Magn. Reson.*, 2004, **171**, 135.
23. P. Lesot and O. Lafon, *Chem. Phys. Lett.*, 2008, **458**, 219.
24. A. Navarro-Vazquez, P. Berdagué and P. Lesot, *ChemPhysChem.*, 2017, **18**, 1252.
25. P. Lesot, R.R. Gil, P. Berdagué and A. Navarro-Vazquez, *J. Nat. Prod.*, 2020, **83**, 3141.
26. C. Aroulanda, O. Lafon and P. Lesot, *J. Phys. Chem. B.*, 2009, **113**, 10628.
27. O. Lafon, P. Berdagué and P. Lesot, *Phys. Chem. Chem. Phys.*, 2004, **6**, 1080.
28. P. Lesot and O. Lafon, *Anal. Chem.*, 2012, **84**, 4569.
29. P. Tzvetkova and B. Luy, *Magn. Reson. Chem.*, 2016, **54**, 351.
30. B. Gouilleux, A. Meddour and P. Lesot, *ChemPhysChem.*, 2020, **21**, 1548.
31. H. Kovacs, D. Moskau and M. Spraul, *Prog. Nucl. Magn. Reson. Spectrosc.*, 2005, **46**, 131.
32. K. Kazmierczuk, O. Lafon and P. Lesot, *Analyst*, 2014, **139**, 2702.
33. R. Dass, W. Koźmiński and K. Kazmierczuk, *Anal. Chem.*, 2015, **87**, 1337.
34. N. Gouilleux, Charrier, B. Akoka, F.-X. Felpin, M. Rodriguez-Zu-Biri and P. Giraudeau, *TRAC-Trends in Anal. Chem.*, 2016, **83**, 65.
35. F. Dalitz, M. Cudaj, M. Maiwald and G. Guthau, *Prog. Nucl. Magn. Reson.*, 2012, **60**, 52.
36. C. Jacquemmoz, F. Giraud and J.-N. Dumez, *Analyst*, 2020, **145**, 478.
37. W.J. Leigh, M.S. Workentin, D. Demus and V. Vill, Liquid crystals as solvents for spectroscopic, chemical reaction, and gas chromatographic applications. In book: *Handbook of Liquid Crystals Set. D*. Demus, J. Goodby, G.W. Gray, H.-W. Spiess and V. Vill, (Eds.). (2008). DOI: 10.1002/9783527619276.ch9da.
38. M. Chan-Huot, P. Lesot, P. Pelupessy, L. Duma, P. Duchambon, G. Bodenhausen, M.D. Toney, V. Reddy and N. Suryaprakash, *Anal. Chem.*, 2013, **85**, 4694.
39. E. Luchinat, L. Barbieri, M. Cremonini and L. Banci, *J. Biomol. NMR* 2021, **75**, 97.

-
40. C. Griesinger, M. Bennati, H.M. Vieth, C. Luchinat, G. Parigi, P. Höfer, F. Engelke, S.J. Glaser, V. Denysenkov and T.F. Prisner, *Prog. Nucl. Magn. Reson.*, 2012, **64**, 4.
 41. B. Plainchont, P. Berruyer, J.-N. Dumez, S. Jannin and P. Giraudeau, *Anal. Chem.*, 2018, **90**, 3639.
 42. S.J. Elliott, Q. Stern, M. Ceillier, T. El Daraï, S.F. Cousin, O. Cala and S. Jannin, *Prog. Nucl. Magn. Reson.*, 2021, **126-127**, 59.
 43. S. Cai, C. Seu, Z. Kovacs, A.D. Sherry and Y. Chen, *J. Am. Chem. Soc.* 2006, **128**, 13474.
 44. F.-X. Theillet, A. Binolfi, S. Liokatis, S. Verzini and P. Selenko, *J. Biomol. NMR* 2011, **51**, 487.
 45. P. Schanda, H. Van Melckebeke and B. Brutscher, *J. Am. Chem. Soc.*, 2006, **28**, 9042.
 46. L. Mueller. *J. Biomol. NMR* 2008, **42**, 129.
 47. J. Farjon, *Magn. Reson. Chem.*, 2017, **55**, 883.
 48. R.M. Rasia, E. Lescop, J.F. Palatnik, J. Boisbouvier and B. Brutscher, *J. Biomol. NMR*, 2011, **51**, 369.
 49. A.A. Maudsley, R.E. Ernst, *Chem. Phys. Lett.*, 1977, **50**, 368.
 50. M. Mobli and J.C. Hoch, *Prog. Nucl. Magn. Reson. Spectrosc.*, 2014, **83**, 21.
 51. A. Tal and L. Frydman, *Prog. Nucl. Magn. Reson. Spectrosc.*, 2010, **57**, 241.
 52. E. Kupce and R. Freeman. *J. Magn. Reson.*, 2003, **162**, 158.
 53. P. Lesot, K. Kazimierczuk, J. Trebosc, J.-P. Amoureux and O. Lafon, *Magn. Reson. Chem.*, 2015, **53**, 927.
 54. M.R. Palmer, C.L. Suiter, G.E. Henry, J. Rovnyak, J.C. Hoch, T.E. Polenova and D. Rovnyak, *J. Phys. Chem. B*, 2015, **119**, 6502.
 55. J.C.J. Barna, E.D. Laue, M.R. Mayger, J. Skilling and S.J.P. Worrall, *J. Magn. Reson.*, 1987, **73**, 69.
 56. D. Rovnyak, M. Sarcone and Z. Jiang, *Magn. Reson. Chem.*, 2011, **49**, 483.
 57. V.Y. Orekhov, I.V. Ibraghimov and M. Billeter, *J. Biomol. NMR*, 2001, **20**, 49.
 58. S. Sibisi, J. Skilling, R.G. Brereton, E.D. Laue and J. Staunton, *Nature*, 1984, **311**, 446.
 59. C.D. Eads and I. Noda, *J. Am. Chem. Soc.*, 2002, **124**, 1111.
 60. R. Brüschweiler and F. Zhang, *J. Chem. Phys.*, 2004, **120**, 5253.
 61. S.G. Hyberts, D.P. Frueh, H. Arthanari and G. Wagne, *J. Biomol. NMR*, 2009, **45**, 283.
 62. D.J. Holland, M. J. Bostock, L.F. Gladden and D. Nietlispach, *Angew. Chem., Int. Ed.*, 2011, **50**, 6548.
 63. O. Lafon, B. Hu, J.-P. Amoureux and P. Lesot, *Chem. Eur. J.*, 2011, **17**, 6716.
 64. R. Brüschweiler, *J. Chem. Phys.*, 2004, **121**, 409.
 65. N. Trbovic, S. Smirnov, F. Zhang and R. Brüschweiler, *J. Magn. Reson.*, 2004, **171**, 277.
 66. Y. Chen, F. Zhang, D. Snyder, Z. Gan, L. Bruschiweiler-Li and R. Brüschweiler, *J. Biomol. NMR*, 2007, **38**, 73.
 67. K. Kazimierczuk and V. Orekhov, *J. Magn. Reson.*, 2012, **223**, 1-10.
 68. J. Candès, J. Romberg and T. Tao. *IEEE Trans. Info. Theory*, 2006, **52**, 489.
 69. K. Kazimierczuk and V.Y. Orekhov, *Angew. Chem. Int., Ed.*, 2011, **50**, 5556.
 70. L. Frydman, T. Scherf and A. Lupulescu, *Prod. Natl. Acad. Sci. USA*, 2002, **99**, 15858.
 71. P. Pelupessy, *J. Am. Chem. Soc.*, 2002, **125**, 12345.
 72. L. Frydman, A. Lupulescu and T. Scherf, *J. Am. Chem. Soc.*, 2003, **125**, 9204.
 73. Y. Shrot, B. Shapira and L. Frydman, *J. Magn. Reson.*, 2004, **171**, 163.
 74. Y. Shrot and L. Frydman, *J. Chem. Phys.*, 2009, **131**, 224516.
 75. P. Mansfield, *J. Phys. Chem.*, 1977, **10**, 55.
 76. P. Giraudeau and L. Frydman, *Ann. Rev. Anal. Chem.*, 2014, **7**, 129.
 77. B. Gouilleux, L. Rouger and P. Giraudeau, *Ann. Rep. on NMR Spectrosc.*, 2018, **93**, 75.
 78. J.-N. Dumez, *Prog. in Nucl. Magn. Reson. Spectrosc.*, 2018, **109**, 101.
 79. P. Giraudeau, T. Montag, B. Charrier and C.M. Thiele, *Magn. Reson. Chem.*, 2012, **50**, S53.
 80. G. Bodenhausen and D.J. Ruben, *Chem. Phys. Lett.*, 1980, **69**, 185.
 81. P. Giraudeau and S. Akoka, *J. Magn. Reson.*, 2008, **192**, 151.
 82. P. Giraudeau and S. Akoka, *J. Magn. Reson.*, 2010, **205**, 171.
 83. P. Giraudeau, G. Remaud and S. Akoka, *Anal. Chem.*, 2009, **81**, 1, 479.
 84. P. Giraudeau, S. Massou, Y. Robin, E. Cahoreau, J.-C. Portais and S. Akoka, *Anal. Chem.*, 2011, **83**, 3112.
 85. P. Giraudeau, P. Lemeunier, M. Coutand, J.-M. Doux, A. Gilber, G.S. Remaud and S. Akoka, *J. Spectrosc. Dyn.*, 2011, **1**, 2.
 86. A. Herrera, E. Fernández-Valle, R. Martínez-Álvarez, D. Molero Z. D. Pardo, E. Sáez and M. Gal, *Angew. Chem. Int. Ed.*, 2009, **48**, 6274.
 87. Z.D. Pardo, G.L. Olsen, M.E. Fernandez-Valle, L. Frydman, R. Martinez-Alvarez and A. Herrera, *J. Am. Chem. Soc.*, 2012, **134**, 2706.

88. A. Herrera, E. Fernández-Valle, R. Martínez-Álvarez, D. Molero-Vílchez, Z.D. Pardo-Botero and E. Sáez-Barajas, *Magn. Reson. Chem.*, 2015, **53**, 952.
89. P. Lesot, P. Berdagué and P. Giraudeau, *Chem. Commun.*, 2016, **52**, 2122.
90. D. Merlet, M. Sarfati, B. Ancian, J. Courtieu and P. Lesot, *Phys. Chem. Chem. Phys.*, 2000, **2**, 2283.
91. A. Le Guennec, P. Giraudeau, S. Caldarelli and J.-N. Dumez, *Chem. Commun.*, 2015, **51**, 354.
92. P. Giraudeau, S. A. Akoka, *J. Magn. Reson.*, **2010**, **205**, 171.
93. D. Schulze-Sünninghausen, J. Becker, M.R.M. Koos and B. Luy, *J. Magn. Reson.*, 2017, **281**, 151.
94. A. Enthart, J.C. Freudenberger, J. Furrer, H. Kessler and B. Luy, *J. Magn. Reson.*, 2008, **192**, 314.
95. D. Schulze-Sünninghausen, J. Becker and B. Luy *J. Am. Chem. Soc.*, 2014, **136**, 1242.
96. E. Kupce and R. Freeman *Magn. Reson. Chem.* 2007, **45**, 2.
97. S. Xiang, V. Chevelkov, S. Becker, A. Lange *J. Biomol. NMR*, 2014, **60**, 85.
98. O. Lafon, J. Trébosc, B. Hu, G. De Paëpe and J.-P. Amoureux. *Chem. Commun.*, 2011, **47**, 6930.
99. S. Paramasivam, C.L. Suiter, G. Hou, S. Sun, M. Palmer, J.C. Hoch, D. Rovnyak and T. Polenova, *J. Phys. Chem. B.*, 2012, **116**, 7416.
100. E.C. Lin and S.J. Opella, *J. Magn. Reson.*, 2013, **237**, 40.
101. S. Sun, S. Yan, C. Guo, M. L, J.C. Hoch, J.C. Williams and T. Polenova, *J. Phys. Chem. B*, 2012, **116**, 46, 13585.
102. G. Porat and A. Goldbourt, *Isr. Chem. J.*, 2019, **9**, 1027.
103. A. Sasaki, J. Trébosc and J.-P. Amoureux *J. Magn. Reson.*, 2021, **333**, 107093.
104. J.S. Gómez, A. G. M. Rankin, J. Trébosc, F. Pourpoint, Y. Tsutsumi, H. Nagashima, O. Lafon and J.-P. Amoureux, *Magn. Reson.*, 2021, **2**, 447.
105. J. Ashida, E. Kupce, J.-P. Amoureux, *J. Magn. Reson.*, 2006, **129**, 129.
106. E. Kupce, J. Trébosc, B. Perrone, O. Lafon and J.-P. Amoureux, *J. Magn. Reson.*, 2018, **288**, 76.
107. P. Paluch, E. Kupce and J.-P. Amoureux, *Magn. Reson. Chem.*, 2021, **59**, 247.
108. M. Gal, C. Melian, D.E. Demco, B. Blümich and L. Frydman, *Chem. Phys. Lett.*, 2008, **459**, 188.
109. M. André, M. Piotto, S. Caldarelli and J.-N. Dumez, *Analyst*, 2015, **140**, 3942.
110. L. Rouger, M. Yon, V. Sarou-Kanian, F. Fayon, J.-N. Dumez and P. Giraudeau, *J. Magn. Reson.*, 2017, **277**, 30.
111. R. Bhattacharyya and L. Frydman, *J. Am. Chem. Soc.*, 2006, **128**, 16014.